Sequence stratigraphic analyses of the interaction between tectonically driven sedimentation and sediment transporting bottom currents in the foreland basin of the Rifian Corridor

Case study from the Gharb and Saïss basins, northern Morocco

W. de Weger
Department of Geology, Utrecht University

(Master Thesis - 2015)

Supervisors: W. Capella, W. Krijgsman & J. Trabucho Alexandre

Abstract

The Rifian Corridor was one of the main marine connections between the Atlantic and the Mediterranean before the Messinian Salinity Crisis (5.97 – 5.33). Previous studies indicated that the Mediterranean became partially isolated from the Atlantic already at 6.64 – 6.44 Ma because of the restriction of this marine connection. The gradual closure of the Rifian Corridor however has been hardly captured stratigraphically since the latest marine deposits are often eroded. In order to specify the processes leading to the closure of the Rifian Corridor a field study was conducted in the Saïss Basin and in the western end of the Gharb basin, located in the mid-western part of the Rifian Corridor. Magnetostratigraphic, biostratigraphic and grain-size results are presented in combination with a sedimentary log of the Neogene deposits at two study-locations near Meknes. Grain-size results are used to correlate and interpret both study-locations. Correlation of the biostratigraphy and polarity sequence of the marl intervals allows an accurate dating of the composite section. The composite section shows an increase in depth related to basin subsidence and is dated at 6.37 – 6.29 Ma. The turbiditic dominated successions show periodic variances in tectonic activity of the source area while subsidence further affected the type of active sedimentary processes. This study furthermore shows increasing influences of bottom current controlled deposits higher up the stratigraphy, indicating changes in the exchange of Atlantic-Mediterranean bottom sea-water. Both sections show different bottom current regimes, the northern section indicates bi-directional flow (E–W & W-E) whereas the southern section indicates dominantly Mediterranean inflow (W–E). The differences in flow regime observed, can be explained by the effect of Coriolis force acting on the water masses in the Rifian Corridor. This theory however enables two scenarios contrasting to present assumptions: 1) another corridor was open and the corridor comprising the study areas was the shallower of the two connections or 2) at the time of deposition, the Rifian Corridor was wider than the assumed width.

Keywords: *Messinian; Morocco; stratigraphy, biostratigraphy, magnetostratigraphy; grain-size analyses; Rifian Corridor; Saïss, Gharb; contourites.*

TABLE OF CONTENTS

INTRODUCTION

The motivation behind this thesis lies in the subject of the Mediterranean salinity crisis (MSC). The discovery of the Mediterranean Evaporite sequence by core-drilling from Glomar Challenger in 1970 proved that a massive, more than one km thick salt deposit exists under the deep-sea floor of the Mediterranean *(Hsü et al., 1973)*. From the results of this exploration it was demonstrated that giant salt deposits could have been formed within a relatively short geological time period *(Hsü, 1972)*. Catastrophic changes of environments in a region over 2.5 million km^2 have been implied from the almost synchronous onset and termination of the MSC *(Hsü et al., 1977; Krijgsman et al., 1999)*.

The onset of the MSC is rooted some 8 million years ago, when the geology and geography of the western Mediterranean differed drastically from the present setting. Eight million years ago, the Strait of Gibraltar did not exist. Alternatively, the Atlantic and Mediterranean were connected by the Betic Corridor through southern Spain and the Rifian Corridor through northern Morocco (**Fig. 1.b**). Gradual closure of both corridors over several million years led to isolation of the Mediterranean.

Studies of *Krijgsman et al. (1999)* dated the synchronous onset of the MCD at 5.96 ± 0.02 million years, whereas the isolation from the Atlantic Ocean was established between 6.64 and 6.44 million years. Isolation of the Mediterranean resulted in a large drop in water-level, followed by erosion (5.59 – 5.50 million years ago) and deposition of non-marine sediments in a large 'Lago Mare' like basin. Their study was in favor of a dominantly tectonic origin for the MSC, although they argue that the exact timing may well have been controlled by the Earth's eccentricity cycle.

Rouchy and Caruso (2006) reassessed MSC data and applied an integrated scenario of the MSC in the Mediterranean basin. They stated that the restriction of the Mediterranean was predominantly under a tectonic control, but the complex development of the evaporitic crisis implied the interplay of both glacio-eustatic changes and fluctuations of the circum-Mediterranean climate. Furthermore, they stated that reduced inputs of seawater continued to enter at least episodically the basin through the MSC, explaining the sporadic presence of marine organisms. Atlantic sea-water input values practically ceased during the latest Messinian, indicating complete closure of both corridors at that time - just before the abrupt restoration of stable open marine conditions at the beginning of the Zanclean.

A group of *MEDGATE* researchers are studying the extraordinary event of the MSC, trying to reconstruct the detail of events leading to the MSC and how the catastrophic changes in Mediterranean seawater impacted the local regional and global climate.

In contribution to the *MEDGATE* project, an exploration- and field study is executed in the Saïss Basin, located in northern Morocco, positioned in the area of the Rifian Corridor. This study focusses on capturing and dating the sedimentary succession related to the gradual closure of the Rifian Corridor.

The sedimentary succession related to the closure of the Rifian Corridor will provide insight in the events an processes leading to the MSC. Since marine gateways play a critical role in water-exchange, heat, salt and nutrients between oceans and seas, this study will provide the ability to further investigate water-exchange between the Atlantic Ocean and the Mediterranean and to quantify the relative significance of water-exchange between the Rifian Corridor and the Betic Corridor. Understanding of the events, exchange through the gateway and the process of gateway restriction and closure aids not only ongoing and future studies related to the processes and effects of the MSC, but can be beneficial for all gateway related studies.

Fig. 1.a *Geological map showing the location and geometry of both the Betic- and Rifian Corridor reconstructed by Ivanovic et al. (2013) (based on Santisteban and Taberner, 1983). Main study area location indicated by blue dots.*

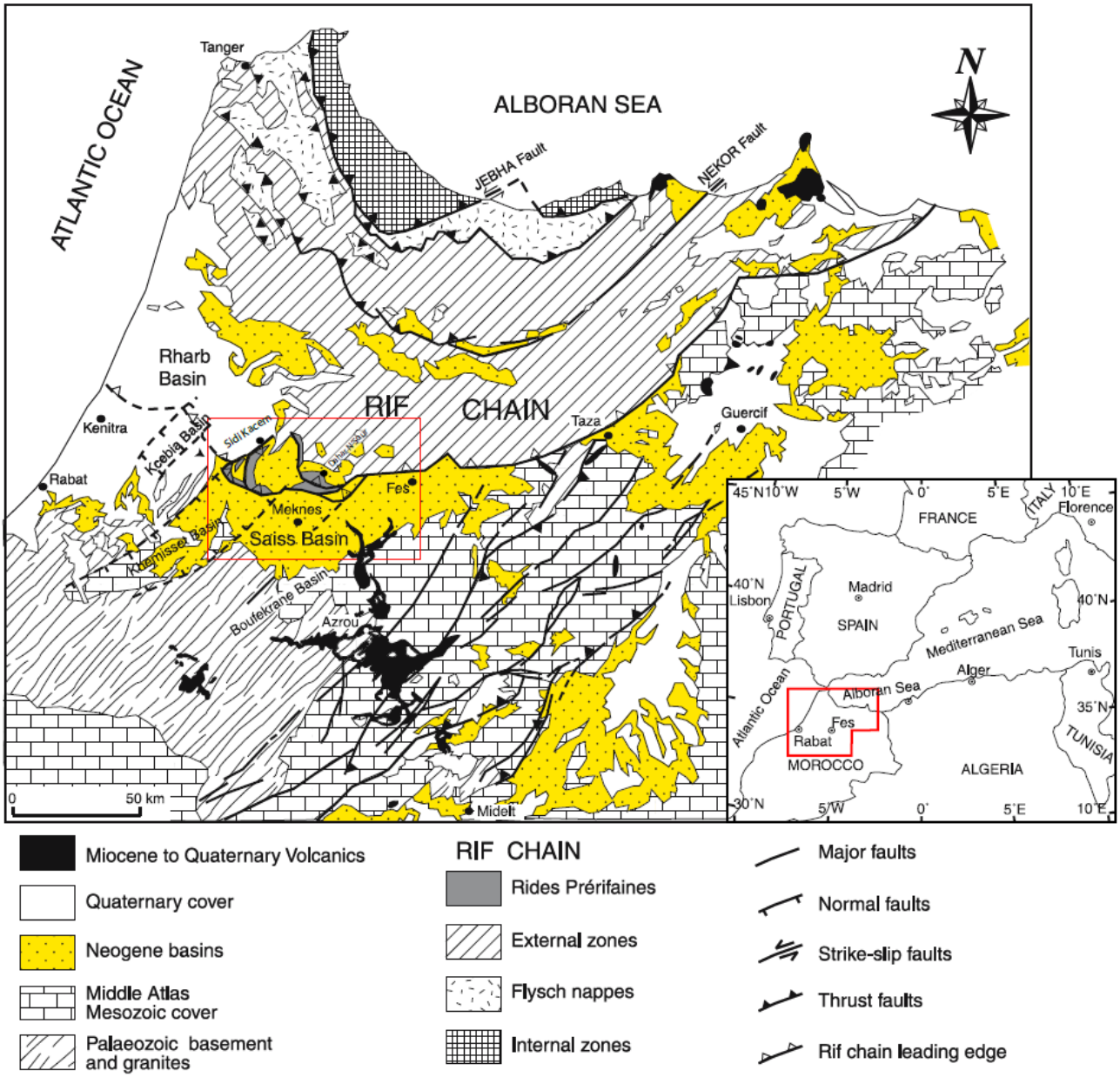

Fig. 1.b *Geological map of northern Morocco. In red, the location of the study area. The map and subdivisions of the structural units are derived from Sani et al. (2007) who derived the figure following findings of Michard (1976) and the Carte Géologique du Maroc (1985).*

1. GEOLOGICAL SETTING

The Rides Prerifaines *(RP; Daguin 1927)* of Morocco form the leading edge of the Rif chain (**Fig. 1.b**). Works of *(Zizi 1996a, b, 2002; Frizone de Lamotte et al. 2004)* show that a deep, flat structure of almost peneplained Palaeozoic substratum is positioned beneath a Triassic-Palaeocene succession. In Early Mesozoic NE-SW-trending basins were formed by rifting, creating accommodation space for a Triassic syn-rift fluvial successions (continental Triassic redbeds), overlain by 500-1,000 m of anhydritic and halitic evaporites interbedded with basalts and dolomites of Triassic-Hettangian age *(Sani et. al., 2007)*. Rifting continued during Pliensbachian to Bajocian resulting in the deposition of a shallow to deep marine syn-rift sequence. The rifting stage terminated in the Middle-Late Jurassic *(Sani et. al., 2007)*.

The base of a thin middle to upper Cretaceous sequence, which is only exposed in the Dahar N'sour area (**Fig. 1.b**) – located approximately 18 km north to north-east of Meknes, *(Bruderer et al. 1950b; Tilloy 1955; Chenakeb 2004)* is separated from Middle-Late Jurassic deposits by a significant hiatus (**Fig. 2**). *Faugeres, 1978, 1981 and Zizi 2002* indicated that

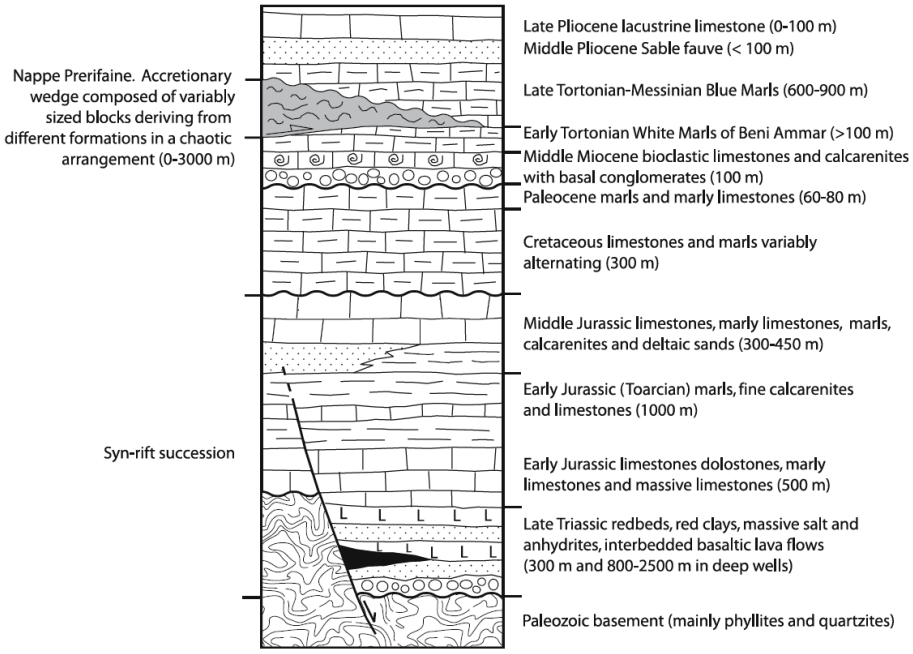

Fig. 2 *Composite stratigraphic-column of the Mesozoic and Tertiary rocks of the Saïss Basin. From Sani et al. (2007). (Note: not to scale)*

the Cretaceous and Paleocene sequence may represent a gulf (with limestones and marls), whilst other parts of the present RP emerged *(Sani et al., 2007)*.

Paleocene marls and marly limestones form the base of a thin unconformable sequence of Middle Miocene to Late Pliocene foredeep deposits. Wedged within this foredeep succession, which mainly consists of Beni Ammar White Marls and the Blue Marl Formation *(Sani et al., 2007),* is the accretionary complex of the pre-Riffian nappe (thin-skinned deformation) (**Fig. 3**). The accretionary complex consists of a mélange of different lithologies, mainly composed of limestones, sandstones and evaporates mixed with soft sediments, which are remnants of the foredeep succession. The thin-skinned emplacement of the Prerifian nappe allows for a division of pre-nappe foredeep succession (Beni Ammar White Marls) and a post-nappe foredeep succession (Blue Marl Formation). The pre-rifian nappe emplacement within the foredeep is dated from the latest Tortonian-Messinian in the area of the Saiss basin to Pliocene in the Gharb basin (Sani et. al., 2007).

The post-nappe blue marls consist of fine sediments with a majority of silt, containing some in-situ bivalves and echinoderms. The blue marls show alternations of clay with a dominant very fine silt content to dominantly clay with medium-silt content. Above the blue marl member an approximately 100 m thick sand rich succession (sandy member of the Blue Marl Fm.) is deposited with locally unconformable deposits of littoral

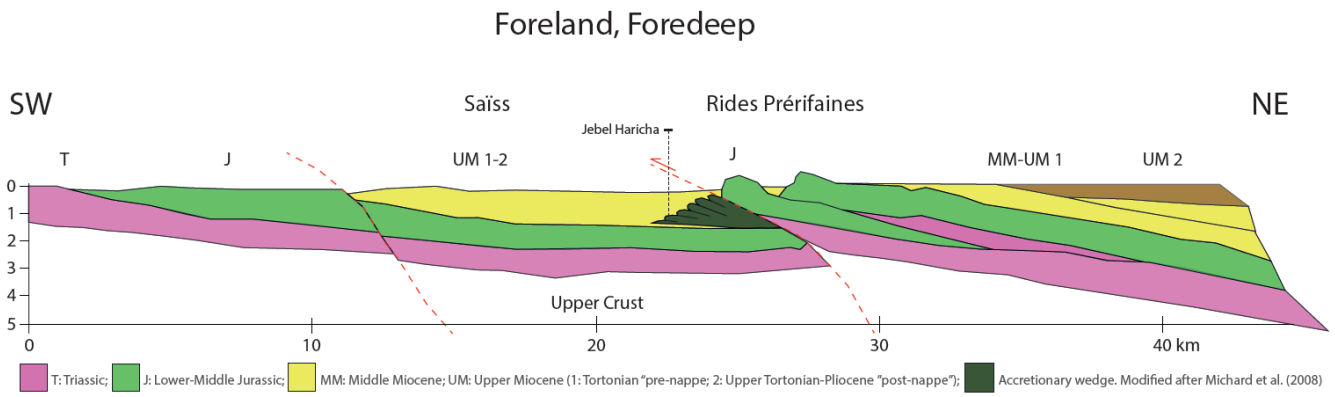

Fig. 3 *NE – SW cross-section indicating the accretionary wedge that formed due to the thin-skinned Nappe emplacement. This cross-sectoion is modified after Michard et al. (2009)*

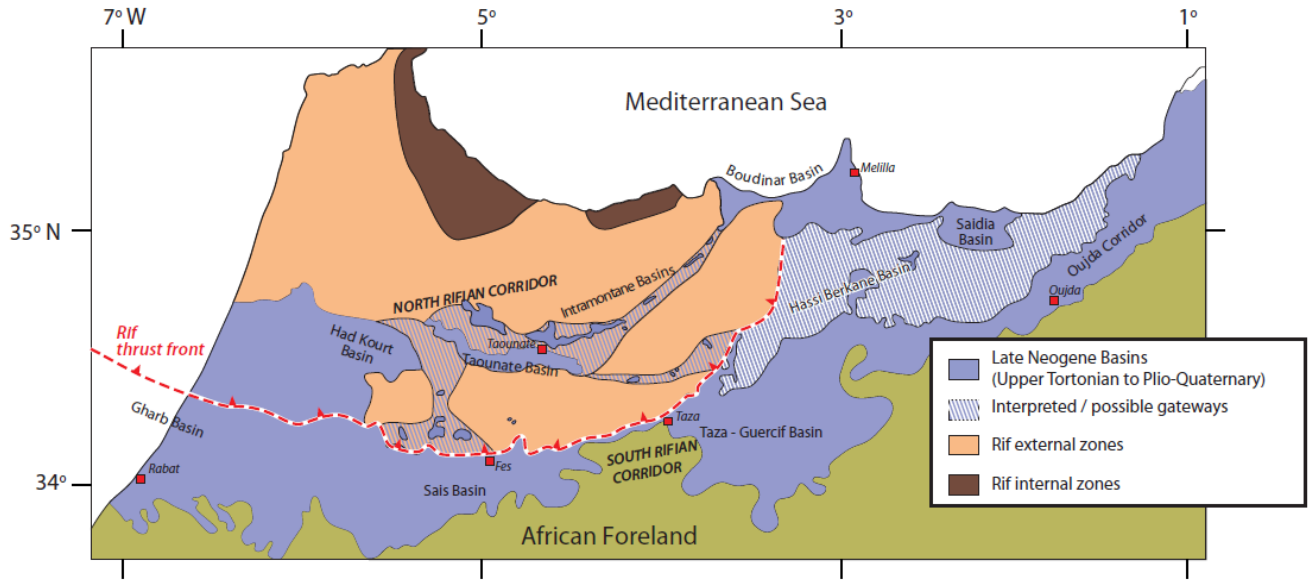

Fig. 4 *Geologic map showing the Rif-zones and the late Neogene basins. The late Neogene basin geometry can serve as an indication of the location of the Rifian Corridor. Constructed by W. Capella (2015).*

sands.

The current morphology of the RP is the consequence of thick-skinned compressive tectonics with an anticlockwise rotation trend *(Sani et al., 2007)*. The major RP ridges coincide with southwest verging thrust faults that are rooted in the basement, but also affect the Neogene foredeep sediments. Major faults strike NE-SW to N-S and mainly SW-SE to E-W *(Sani et al., 2007)*. Frontal ramps of the RP are roughly oriented WNW-ESE, whereas lateral ramps are oriented NE-SW, mainly parallel to the normal faults related to Mesozoic rifting. The RP arcuate geometry in map view is strictly tied to the trends of the graben systems inherited since Late Triassc-Jurassic opening of the central Atlantic Ocean *(Faugeres 1978; Boutakiout 1990; Laville and Piqué 1991; Olsen 1997; Laville et al. 2004; Sani et. al., 2007)*.

During the Late Pliocene, the shallow marine and littoral sands that are exposed in the Dahar N'Sour area were overlain by lacustrine limestones in the Saiss Basin. Taltasse (1953) precisely evaluated the extension of this lacustrine environment, which is one of the most prominent features in the Saïss Basin and has a varying thickness from 10 up to 100 m. At the same time during Late Pliocene, a marine environment dominated to the west and north-west of the Rharb basin. The recent evolution of the area is exhibited by the Pliocene and Quaternary infill, affected by compressional and extensional deformation. In the area near Guerzine (between Fez and Meknes) the Pliocene limestones are deformed by normal NNE-SSW syn-sedimentary faults followed by later en echelon folds with axes of N120°E to N150°E that are said to be related with E-W sinistral faults, and finally reverse faults oriented NE-SW *(Ahmamou and Chalouan, 1988; Bargach et al., 2004)*.

2. SAÏSS-GHARB BASINS

The Saiss-Gharb Basin (or Rharb; *Sani et al., 2007)* extends from the Atlantic eastward to the Taza Strait (**Fig. 4**). The Rharb basins which eventually compose the geometry of the Rifian Corridor, opened in Late Miocene in relation to the collapse of the northern edges of the western Meseta and the Middle Atlas *(Bargach et al., 2004)*. The Gharb basin is located west of the Saiss Basin stretching from the Atlantic coast to Sidi Kacem in the East. The Saiss basin, located roughly south-east of the Gharb Basin contains the towns of Meknes and Fes.

The most important findings of seismic profiles and boreholes carried out in the Gharb basin show that the basement consists of Paleozoic granites followed by a Triassic-Jurassic lacustrine limestone sequence, overlain by a Miocene sequence that is similar for both the Saïss- and Gharb Basins (**Fig. 2**).

The Pliocene sequence of the Gharb Basin shows a marine sequence whereas the Saiss Basin consists of a lacustrine succession. Thrust sheets of Preriffian rocks are intergraded through a series of interlocking or overlapping wedge-shaped layers with Upper Miocene deposits in the eastern

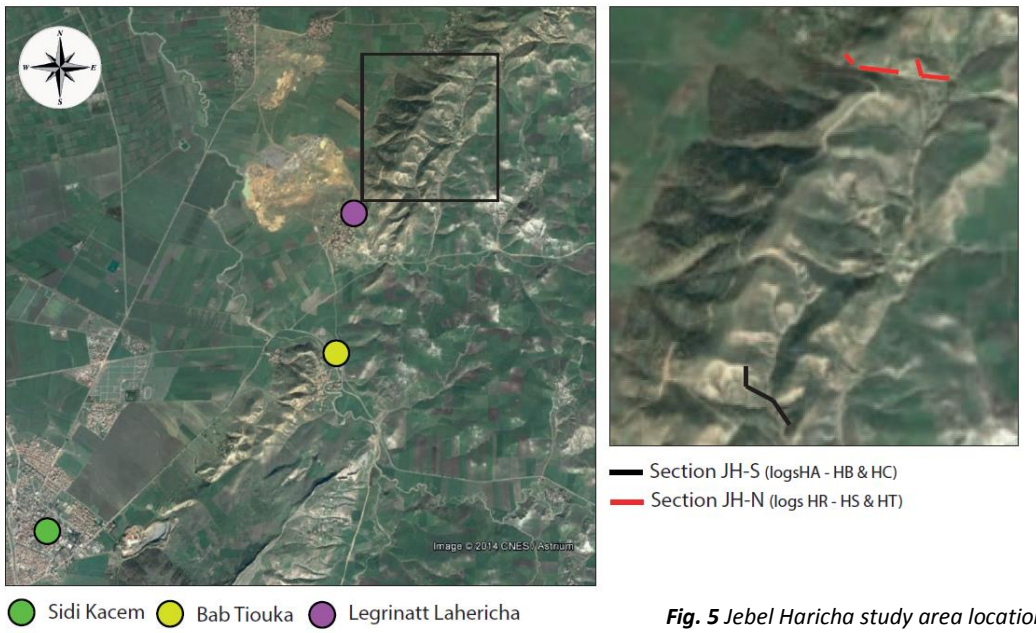

Fig. 5 *Jebel Haricha study area location. Source: Google Earth.*

part of the Gharb Basin, and Pliocene deposits towards the Saiss Basin *(Bargach et al., 2004)*.

During Late Miocene, the Saiss basin acted as a subsiding marine basin whereas in Late Pliocene and Quaternary this basin consisted of a lacustrine environment *(Taltasse, 1953; Feinberg, 1986)*. During the Pliocene, the Gharb Basin underwent rapid subsidence and was simultaneously exposed to thrusting by the Pre-Riffian thrust sheet *(Feinberg, 1986; Flinch, 1996; Litto et al., 2001)*. The northern edge of the Saiss Basin however, was subjected to significant compressive deformation and thrusting of the External Rif and Pre-Riffian ridges *(Bargach et al., 2004)*.

3. STUDY AREAS

We (W. Capella, M. van Oorschot & W. de Weger) arrived in Morocco on the 12th of September 2014. The first 7 days were spend exploring the area around Meknes with the additional supervision of J. Trabucho Alexandre from 15 to 19 September. Our main targets were the area near Sidi Kacem (Jebel Haricha), Bab Tisra, Moulay Idriss, Oued Serra and Moulay Ya Koub - which were mentioned in the ERICO report (1993) (**Appendix 1**). Both Bab Tisra, Moulay Idris, Oued Serra and Moulay Ya Koub - proved not useful due to lack of exposure or continuity whereas the Jebel Haricha section was well exposed and appeared relatively continuous (**Fig. 5**). Driving on the N6 from Fes to Meknes a second suitable study area was discovered in a valley NE of Douar Oued Mahdouma (**Fig. 6**).

- Jebel Haricha -

The Jebel Haricha composite-section is located on top of the pre-riffian nappe on the north-western edge of the Saïss basin and consequently near the south-eastern edge of the Gharb basin. The first part of the study area is situated 7 kilometers north of Sidi Kacem and near the small village of Legrinatt Lahericha. The second part of the study area is located 2 km NE of the 1st part and 1.8 km south of the small village of Ouled Mbarek Bir Taleb (**Fig. 5**). The altitude of the section locations ranges from 130 to 210 m.

- Mahdouma -

The Mahdouma study area is situated north of the N6 between Meknes and Fes and north-east of the small village of Douar Oued Mahdouma (**Fig. 6**). This area, a river incised valley, is split-up in multiple sections covering the majority of decent outcrops in the valley, providing a 3-dimensional coverage of the stratigraphy. The valley lies at an altitude between 350 and 450 meters.

4. METHODS

The fieldwork was conducted by *M. van Oorschot & W. de Weger* under the supervision of *W. Capella. J. Trabucho Alexandre* and *L.C. Matenco* who separately joined us for a couple of days to provide extra supervision and guidance.

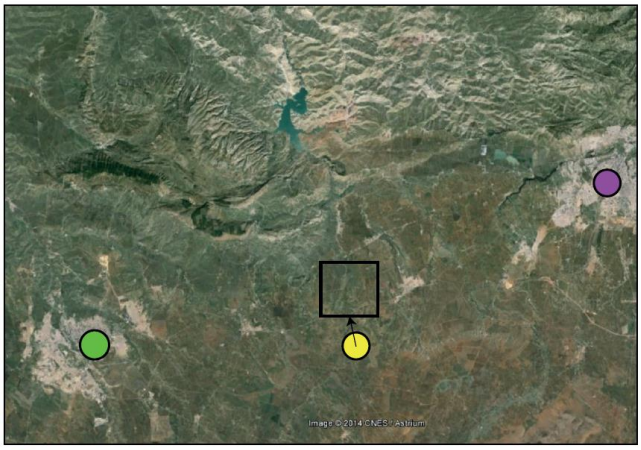

NB: Location of sections are indicative

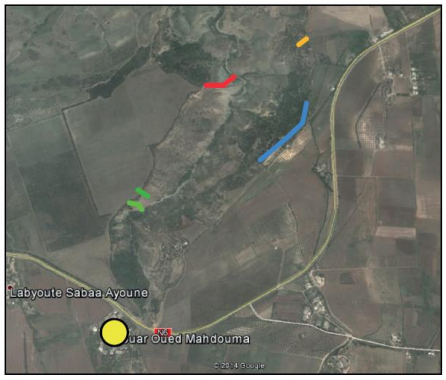

Fig. 6 Mahdouma study area. Source: Google Earth

4.1. Sedimentary logs

The methods conducted for gathering data and evidence on the nature and depositional conditions of the sedimentary rocks in the Saïss Basin include the production of multiple 1:100 scaled logs for the Jebel Haricha sections (JH-S & JH-N) and 1:20 scaled logs for the Mahdouma sections (M-NW, M-SW and M-NE) **(appendix 2)**.

The procedure of logging started by marking absolute thicknesses on the exposed rock using spray paint *(as suggested by J. Trabucho Alexandre)*. Every interval of 5 meters of true stratigraphic thickness was denoted by a straight line along with a number of the total stratigraphic thickness measured so far, each of these intervals was divided into meters by spraying dots. All sedimentary features: bed thickness, bed composition, grain size, sedimentary structures, macrofossil content etcetera, were logged on the spot. Picture numbers, dip directions as well as sample numbers and palaeo-current directions were also directly written on the log sheets. Basic geological tools consisting of: hand lenses, a compass, geological hammers and a measuring tape were used to conduct the field-research.

4.2. Sampling

Sampling was conducted by W. Capella, M. van Oorschot and W. de Weger. Bio-stratigraphic samples were taken every 3 m where possible, mainly in the marl members. Grain-size samples were taken every 10 m, also taking into account the differences in stratigraphy, samples were taken from the finer and coarser beds were they were alternating, sometimes taking multiple samples in one bed where possible grading occurred.

Both types of samples were gathered using; a pick-axe, geological hammers and a hand plow. The samples for magneto-stratigraphy were also taken every 10 m but proved more difficult to collect, since the combination of an electric drill and a water pump did not prove to be very successful in the marls as the drill continuously clogged up by clay-swell. Several cores however were drilled properly, the remaining samples were taken as oriented blocks of which cores were later drilled at Fort-Hoofddijk (Utrecht University) using an electric drill and compressed air.

4.3. Grain size analyses

Samples were taken roughly every 10 m in the stratigraphic record in order to analyze the sedimentary deposits on: grain-size distribution and grain-size alternations. These grain size samples were preferably taken from fresh rock and measured approximately 4-8 cm^3. All the samples were stored in zipper-bags labeled with their section name (Sample type – "G" for grain-size, and their stratigraphic height in the record).

The grain-size samples were cut to a proper size at Utrecht University using a circular power saw. The remaining sample, which measured approximately 1 cm^3 was carefully crushed trying to avoid destruction of individual grains.

The crushed samples where then transferred to a plastic tube with screw lid as

preparation for the addition of acid. Acetic acid was added to dissolve carbonates in the matrix and carbonates possibly coating the grains. At the same time the acids enabled the sample to fall apart separating the sample into individual grains.

The acid consisted of 3M which is 1 part of acid for each 2 parts of ionized water. After having stored the samples for 2 days they were checked for acidity, a pH below 7 indicated that all the carbonate was dissolved. The dissolved samples were put in a centrifuge at 2200 rpm for 15 minutes (excluding the start-up and slowing down time) after which the fluids were disposed of and replaced by fresh ionized water. This procedure was repeated 3 times for every sample to ensure no acid remained.

For the grain size analyses, the *Malvern Mastersizer 2000* located at the GML building of Utrecht University was used. The Mastersizer 2000 uses the technique of later diffraction to measure the size of particles. The intensity of scattered light is measured as a laser beam passes through a dispersed particulate sample. The scattered light data is analyzed to calculate the size of the particles that created the scattering pattern (Malvern website). In order to improve accuracy 3 portions of each sample were fed individually to the Malvern Mastersizer 2000 and PEP was added to enhance the separation of individual grains.

The grain-size results obtained by the Mastersizer 2000 were exported to an excel file containing all necessary data. The results were stored in µm and converted into phi (ϕ) values which are used in the Krumbein grain-size scale (BOX 1). The Krumbein scale is based on the relationship:

$$\phi = -log_2 S$$

where ϕ is phi size and S is grain size in millimeters.

The phi scale is needed to calculate: Graphic mean, Inclusive graphic standard deviation, Inclusive graphic skewness and the Graphic kurtosis (BOX 1).

The mean size is the arithmetic average of all the particle sizes in a sample. The true arithmetic mean size of all the grains in a sediment sample cannot be calculated from the data

BOX 1.

The Krumbein *Phi* (ϕ) scale, a modification of the Wentworth scalecreated by *W.C. Krumbein in 1937*, is a logarithmic scale. Each value in this scale is either two times larger than the preceding value or one-half as large, depending upon the sense of direction. The Udden-Wenthworth scale, most widely used by sedimentologists, *(Wentworth, 1992)* extends from < 1/256 mm to > 256 mm and is divided into four major size categories (clay, silt, sand, and gravel) (Table 1).

Millimeters	µm	Phi (ϕ)	Wentworth size class	
		-20		
4096		-12	Boulder (-8 to -12ϕ)	
1024		-10		
256		-8	Pebble (-6 to -8ϕ)	
64		-6		
16		-4	Pebble (-2 to -6ϕ)	
4		-2		Gravel
3.36		-1.75		
2.83		-1.50	Gravel	
2.38		-1.25		
2.00		-1.00		
1.68		-0.75		
1.41		-0.50	Very coarse sand	
1.19		-0.25		
1.00		-0.00		
0.84		0.25		
0.71		0.50	Coarse sand	
0.59		0.75		
1/2 – 0.50	500	1.00		
0.42	420	1.25		
0.35	350	1.50	Medium sand	Sand
0.30	300	1.75		
1/4 – 0.25	250	2.00		
0.210	210	2.25		
0.177	177	2.50	Fine sand	
0.149	149	2.75		
1/8 – 0.125	125	3.00		
0.105	105	3.25		
0.088	88	3.50	Very fine sand	
0.074	74	3.75		
1/16 – 0.0625	63	4.00		
0.0530	53	4.25		
0.0440	44	4.50	Coarse silt	
0.0370	37	4.75		
1/32 – 0.0310	31	5	Medium silt	
1/64 0.0156	15.6	6	Fine silt	
1/128 0.0078	7.8	7	Very fine silt	
1/256 – 0.0039	3.9	8		Mud
0.0020	2.0	9		
0.00098	0.98	10		
0.00049	0.49	11	Clay	
0.00024	0.24	12		
0.00012	0.12	13		
0.00006	0.06	14		

Table 1. Udden-Wenthworth scale (1922)

The mean size is the arithmetic average of all the particle sizes in a sample. The sorting of a grain population is a measure of the range of grain sizes present and the magnitude of the spread or scatter of these sizes around the mean size. The mathematical expression of sorting is standard deviation (σ). In conventional statistics, one standard deviation encompasses approximately the central 68 percent of the area under the frequency curve *(Fig. 1)*. Skewness (SK) is an additional measure of grain-size sorting that reflects sorting in the tails of the distribution. When plotted as a frequency curve the grain-size distributions of most natural sediments do not yield a perfect bell-shaped curve such as the idealized curve shown in Fig. 1. That is, they do not exhibit a normal, or log-normal, grain-size distribution. Instead, they display an asymmetrical or skewed distribution (Fig. 2).

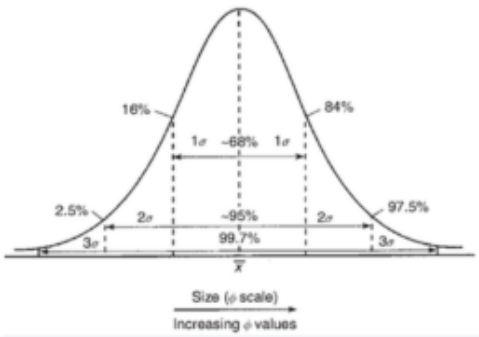

Fig. 1 Frequency curve for a normal distribution

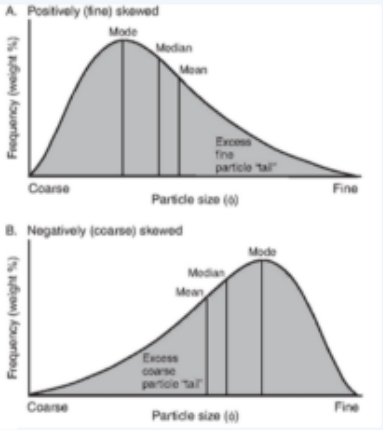

Fig. 2 Skewed grain-size frequency curves

(NOTE: All information provided in this box is directly copied from Boggs, Jr. 2009)

obtained. An approximation of the mean size is calculated from the formula:

$$M_z = \frac{\phi 16 + \phi 50 + \phi 84}{3}$$

where M_z is the graphic mean and ϕ16, ϕ50 and ϕ84 are the 16th, 50th and 84th percentile diameters determined from cumulative values.

The sorting of a grain size sample is a measure of the range of grain sizes present and the magnitude of the spread or scatter of the sizes around the mean size. A formula for calculating the approximate standard deviation of a grain-size distribution by graphical-statistical methods is used to yield the standard deviation expressed in phi units. The formula used to determine the Inclusive graphic standard deviation is

$$\sigma_i = \frac{\phi 84 - \phi 16}{4} + \frac{\phi 95 - \phi 5}{6.6}$$

Skewness is an additional measure of grain-size sorting that focusses on the sorting in the far ends of the distribution curve. When the excess of fine particles is present, the distribution is said to be fine-skewed (positive phi values), and vice versa, when there is an excess of coarse particles the distribution is coarse-skewed and has negative phi values. The numerical value of skewness can be calculated using:

$$SK_i = \frac{(\phi 84 + \phi 16 - 2\phi 50)}{2(\phi 84 - \phi 16)} + \frac{(\phi 95 + \phi 5 - 2\phi 50)}{n(\phi 95 + \phi 5)}$$

The sharpness of a grain-size frequency curve is referred to as kurtosis. Sharp peaked curves indicate better sorting in the central portion of the grain-size distribution than at the far ends, flat-peaked curves indicate the opposite. The kurtosis is calculated by:

$$K_G = \frac{(\phi 95 - \phi 5)}{2.44\,(\phi 75 - \phi 25)}$$

(The information concerning grain size calculations is obtained from Folk, R.L. and W.C. Ward, 1957. Background information has been deducted from Boggs, S).

4.4. Thin sections

During the fieldtrip, 19 samples were collected for the use of microscope petrology. The samples were first cut to a proper size and shape after which they were prepared to be grinded to a thickness of 30 µm. The majority of the samples are marked by their stratigraphic upward direction in order to facilitate the study of fining directions. The samples were analyzed using a petrographic microscope and photographed using a webcam and scanner.

4.5. Magnetostratigraphy

Magnetostratigraphy is used for dating the sedimentary succession, accurate time control is used to understand rates of change of sedimentary processes.

The primary natural remanent magnetization (NRM), in this case the magnetization that originated at the time of rock formation can be overprinted by magnetic components that have been acquired through weathering reactions or thermochemical reactions associated with tectonic burial processes *(Langereis et al., 2010)*. In this case, the overprint components have been removed using the thermal demagnetization technique.

During this analysis, conducted at Fort Hoofddijk (Utrecht University), samples are subjected to stepwise increasing values of temperature in a zero magnetic field space (2G Enterprises DC-SQUID magnetometer). Residual magnetization is measured after each temperature- (demagnetization) step and the resultant changes in direction and intensity are displayed and analyzed in order to reconstruct the complete component structure of the NRM *(Langereis et al., 2010).*

The results of this stepwise demagnetization are visualized and analyzed using the so-called *Zijderveld diagrams (after Zijderveld 1967)*.

4.6. Biostratigraphy

Bio-stratigraphic sampling has been conducted at 4 locations mainly in the marls. Two of those sites are located in the Jebel Haricha sections (JH–S & JH-N) and two in the Mahdouma area (M-NW & M-SW). bio-stratigraphic samples have been taken at three meter intervals where possible in the marls. Samples from the sand rich member have been sampled only in the finest grained beds.

Bio-stratigraphic analysis of the Jebel Haricha composite-section has been carried out by *Phd. M.A. Tulbure*, the results of the Mahdouma area however remain to be studied.

A semi quantitative analysis of potential

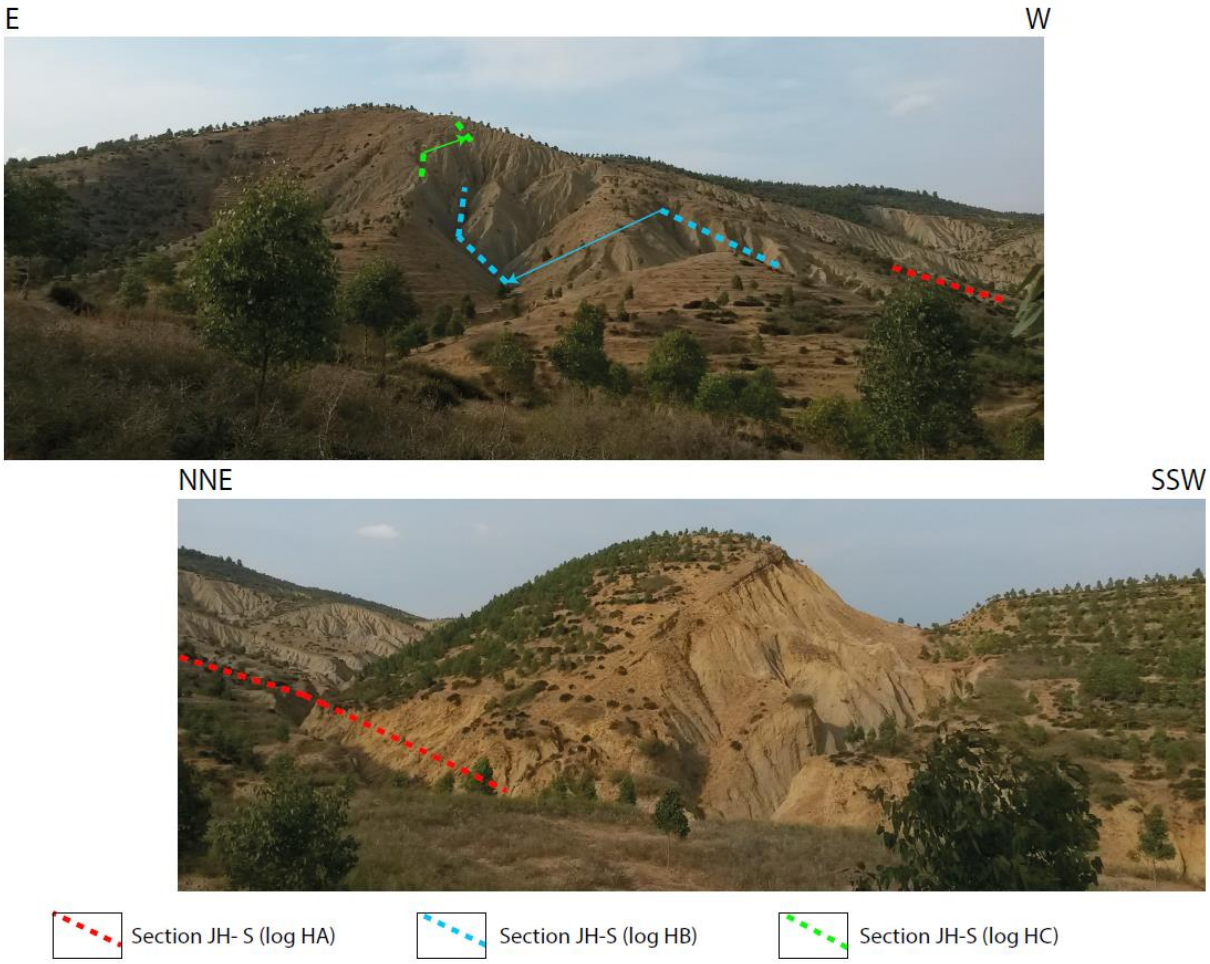

Fig. 7 *Overview of the location of section JH-S, composed of logs HA, HB and HC. Note that there are only small offsets between the logs, enhancing the ability to correlate. NB; the red dotted line indicating section HA is continuous from one picture to the other.*

marker species was carried out on the >125 mm fraction of the washed residue for 56 samples from the sections JH-S and JH-N. In normal tray marker species were counted in 15 squares. The distribution of the marker species was divided in the following groups: trace (0-5), common (5-15), abundant (15-35), acme (>35).

In addition, the coiling direction of the neogloboquadrinids was determined. The distribution of these six species is based on surveying a standard number of fields (15 out of 45) on a rectangular picking tray and specified in qualitative terms (presence, absence) for the Jebel Haricha section.

5. RESULTS

5.1. Sedimentary logs

- Jebel Haricha -

The composite section of the Jebel Haricha study area is composed of five logs (**Fig. 7 & 8**). The stratigraphic base of the composite section, is the base of section JH-S (log HA). Slight lateral location changes (logs HB & HC) have been made to construct a continuous section which is composed of logs H-ABC, which is called section Jebel Haricha – south (JH-S). As stated before, the second part of the Jebel Haricha composite section, section Jebel Haricha – north (JH-N) is located 2 km NE of section JH-S (**Fig. 9**), and is composed of logs HR, HS and HT (**Fig. 8**). Log HT however is not properly documented since the correlation with the rest of the sections is not clear, for this reason has log HT not been taken into account in the composite section of the Jebel Haricha study area, but will be separately discussed.

The most striking feature of the appearance of all both sections is the apparent lack of changes in grain-size distribution. Throughout the section only minor changes in grain-size distribution occur and the majority of the beds are poorly- to very poorly- sorted. Since

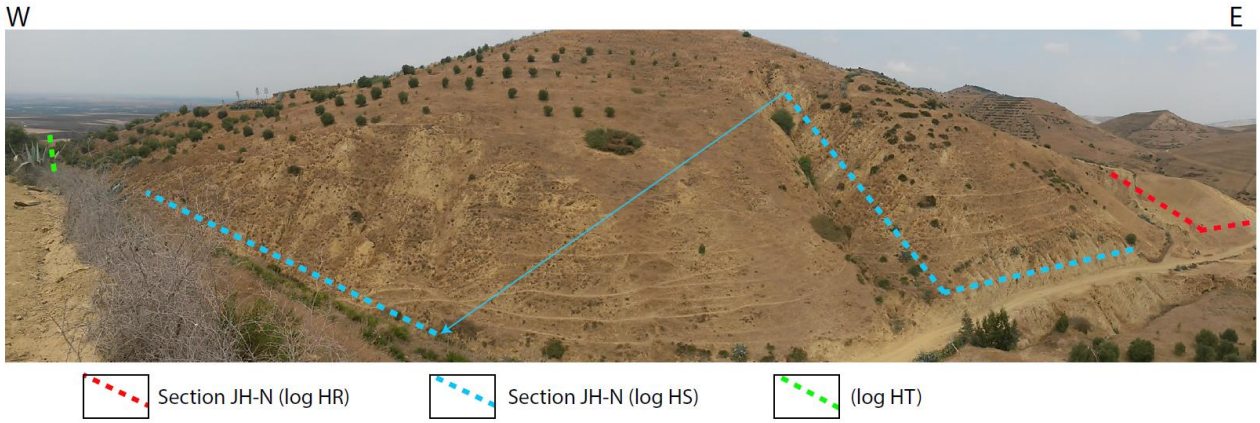

Fig. 8 *Overview of the location were section JH-N was constructed from logs HR and HS. The location of log HT is also indicated. NB; Log HR continues further to the east, the western part of log HS (upper part of section JH-N) is not up-hill but follows the road. Section HT is also situated along the road but this is not shown in this figure (location is indicative) – Furthermore this is a panoramic picture and hence the middle part of the picture appears relatively to close.*

the grain-size variations were nearly invisible during the field-trip, it was very hard to recognize fining trends and sedimentary structures.

The sedimentary logs can be found in ***Appendix 8*** and a summarized version of the logs, only showing 4 types of lithology's can be found in ***Fig. 9*** .

The results of the measured dip directions and palaeo-current directions along with the stratigraphic thickness at the site of the measure-ment are shown in ***table 1*** and reconstructed, rotated palaeo-current directions can be found in **Fig. 24**.

Fossils found were carefully logged and photographed. An overview of the species was send to *F. Wesselingh* who helped identifying them. The resultant fossil overview and palaeo-environmental interpretations can be found in **Appendix 3**.

The total thickness of section JH-S (**Fig. 9**) comprises 251 m of marine deposits. The bottom part of this section, up to 74 m of log Ha consists of sand silt alternations. The sandstones in this part of the section are distinct from sandstones further up the stratigraphy mainly by color. The majority of these sandstones is colored slightly to moderately purple, often containing heavily bioturbated tops in which burrows of Rhyzo-corallium have been identified.

The siltstones, containing variable fractions of clay were predominantly light to darker shades of grey also containing variable amounts of heavy minerals mainly consisting of pyritic raspberries.

At 90 meters up in the stratigraphic record the blue marls appear on top of grey to brown silt deposits. The blue Marls are mainly logged in section HB (HB 0 correlates to 140 m of total stratigraphic thickness – "140 m from the base of JH-S") and contained a variety of fossils, mainly bivalves and a few echinoderms.

This fine grained member of the Blue Marl Fm. consists of blueish marls with alternating silt content. A sharp contact separates the blue marls with the next member of the Blue Marl Fm., consisting of grey silty marls interbedded with reddish sandbeds. This occurs at 205.5 m total stratigraphic thickness, correlating to the beginning of log HC (HC 2.8 correlates to HB 65.5 at a total stratigraphic thickness of 209.3 m in section JH-S).

Log HC, the upper part of section JH-S, is marked by an alternation of grey siltstones and red sandbeds which showed different kinds of laminations (parallel, cross and wavy- laminated), erosional surfaces (scour marks) and signs of soft sediment deformation.

A distinct feature of this part of the section were the iron concreted layers occurring on the tops and bottoms of the sand beds, which were often heavily bioturbated. The dominant fossil in this area is the pecten.

Since sections JH-S and JH-N (**Fig. 9**) are not easily correlated by sight, care has been taken to create significant overlap in order to correlate both sections with the help of other data such as bio-, magneto-stratigraphy and grain-size analyses. For this reason, the base of section JH-N lies way down in the blue marl member. The total stratigraphic thickness of section JH-N is 328 m. At a stratigraphic thickness of 142 m above the base

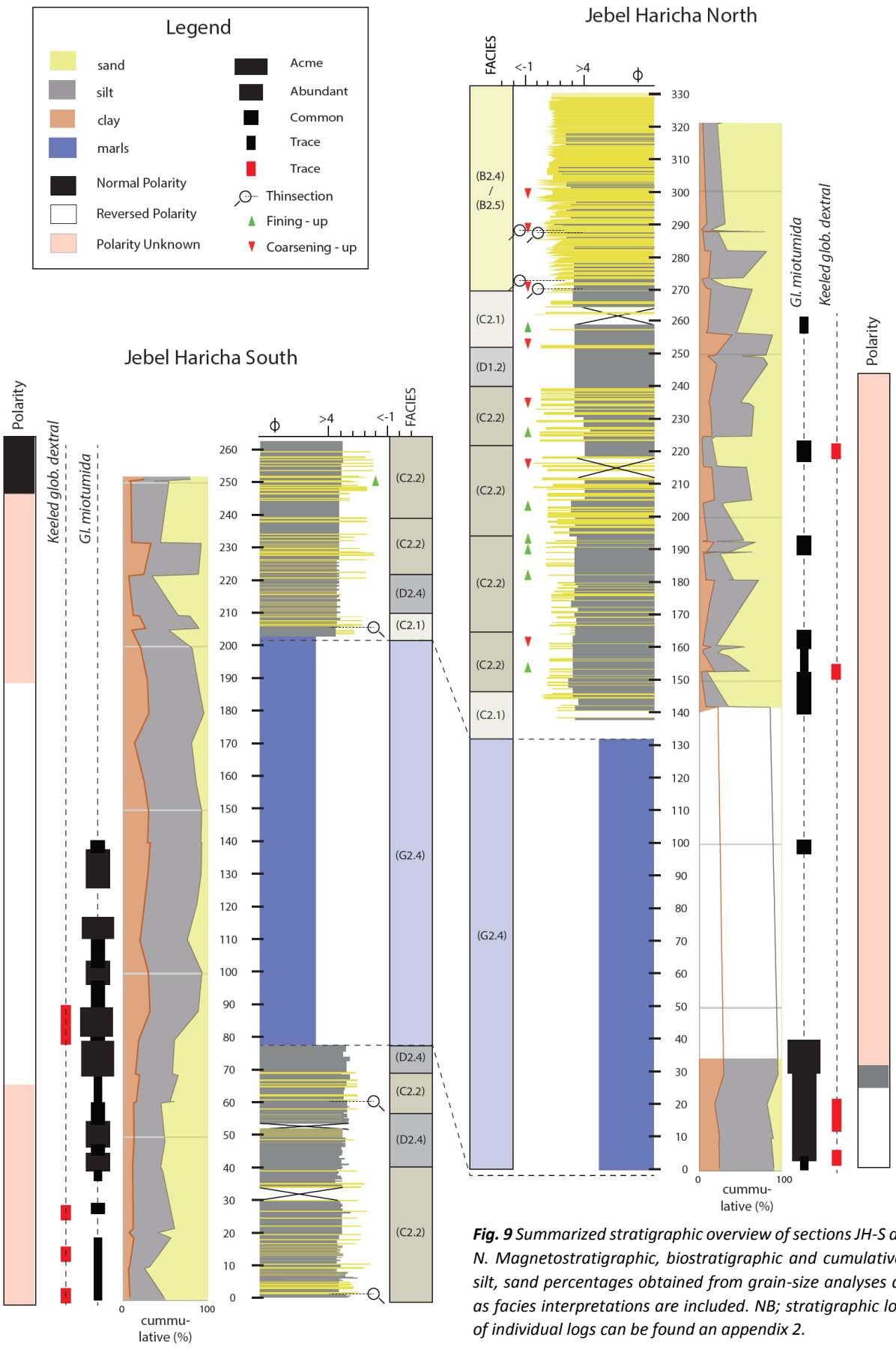

Fig. 9 *Summarized stratigraphic overview of sections JH-S and JH-N. Magnetostratigraphic, biostratigraphic and cumulative clay, silt, sand percentages obtained from grain-size analyses as well as facies interpretations are included. NB; stratigraphic location of individual logs can be found an appendix 2.*

Site JH-S (m)	Dip-direction	Palaeo-current direction
2	38 – 310 NW	
20	38 – 290 NW	213 N
22		045 SW
34	28 – 310 NW	350 S
35		23 – 300 N 28 – 270 N 34 – 268 N
43	39 – 299 NW	
69	40 – 312 NW	
206		031 S
209	35 – 293 NW	
223		035 SW
230		015 S
233		010 S
246	30 – 287 NW	015 NW
247		031 SW
252		019 S

Site JH-N (m)	Dip-direction	Palaeo-current direction
145		013
155	45 – 310 NW	
170	50 – 325 NW	058
174		024 045
223	45 – 304 NW	099
265	44 – 295 NW	096 W
271		26 – 056 W
272		25 – 044 SW
276	47 – 123 NW	
277		S
280	36 – 303 NW	
284	32 – 300 NW	52 – 175 45 – 185 N 55 - 146
285		42 – 000 N 25 – 121 25 – 134 39 – 146
287	46 – 310 NW	38 – 095
288	44 – 310 NW	
290		35 – 158 NW
296	29 – 310 NW	
297	30 – 326 NW	
299	26 – 333 NW	
304	44 – 311 NW	21 – 064 NW
307	30 – 091	
112	51 – 310 NW	
116		50 – 100 W 50 – 100 E
326	45 – 304 NW	42 – 089 NW

Table 1*. (Above) Dip-direction of the bedding and palaeo-current direction of section JH-S. The site of the measurement is given in stratigraphic chronological thickness from the base at log HA-0.*
(Right) Dip-direction of the bedding and palaeo-current direction of section JH-N. The site of the measurement is given in stratigraphic thickness from the base at log HR-0.
Palaeo-current directions have mainly been derived from crossbedding and occasionally from scour marks.

of JH-N lies the beginning of sub-log HS. The base of log HS is located within the sand rich member.

The transition from blue marls happens with alternating siltstones and thin bedded sandstones that are slightly crème to orange colored. Whilst the siltstones are still dominating, the sandstones show erosional features and mainly contain parallel lamination. Some of the sand beds are very crystalline and show only minor bioturbation. Again, we find sand beds with iron concreted tops and bottoms. However, this time the top concretions often contained iron concreted bioturbation.

Towards the top of the section sandstones become dominant, showing both cross- and parallel-laminations and erosional features. At 272 m of total stratigraphic thickness in the JH-N section, silt-sand alternations are almost completely replaced by sand deposits. The sandstone bed thickness has increased and more sedimentary features such as: channels, swaley cross lamination etc. start to appear.

The most striking features in this part of the log are the laminated sub- to well- rounded muddy silt clasts which are rip-up clasts with a possible component of reworking ***(*Fig. 10a*)*** as well as changes in the angle of dip, homogenous grain-sizes and erosional features (**Fig. 10b**).

Dip directions as well as palaeo-current directions for the Jebel Haricha section can be found in **table 1** and reconstructed, rotated palaeo-current directions can be found in **Fig. 24**.

As stated before, the correlation between logs HS and HT is unclear. The end of section JH-N is located at a GPS position of 34.28670,-5.64618 and the dip direction of the last measurable bed is 52° towards 280° NW, whereas the beginning of section HT is located at a GPS position of 34.28670,-5.64669 and a dip direction of 57° towards 305° NW. Section HS and HT are separated by a gully and lie approximately 30 meters apart without any exposure in-between.

Figure 11 shows a panoramic picture of the 23 m thick HT section. The section starts with a yellow to reddish silt, after which the mean grain-size rapidly increases towards a sandstone which is mainly bright yellow or orange-red colored.

***Fig. 10 a**. (left) Picture containing the laminated silty rip-up clasts found in the upper part of the JH-N section (280m). **b**. (right) Picture of the apparent massive sand deposits found in the upper part of the JH-N section (from 300 m). At first glance the deposits appear very well sorted, grain-size analyses however indicated moderate to very poorly sorted deposits.*

At 17 m in the stratigraphy two thick (4m and 2m) conglomerates appear of which the first has a reddish matrix and is imbricated, and the second has a light matrix with apparently the same pebbles. The imbrication shows a palaeo-current direction of 45° towards 105° NW within the bedding.

Most striking in this short section is an apparent channel which starts at 4.8 m up the stratigraphy. This "channel", which is perfectly rounded at the bottom is filled with conglomeratic material consisting of well-rounded poorly sorted clasts up to 15 cm. Upon closer look, bedding appears to be folded inside and below this feature as interpreted in **figure 11**.

- Mahdouma study area -

The Mahdouma study area is divided in four exploration sites (**Fig. 6 & 12**), three normal stratigraphic logs have been constructed. These stratigraphic logs compose sections M-NW, M-SW and M-NE. The fourth section, section M-SE, has been constructed in a different way. In this section, which is composed of an approximately 300 m long, 4 – 5 m high outcrop with near horizontal dip-direction directions, 4 stops have been conducted in order to specify the statigraphy.

Section M-NW (**Fig. 12**) is located in the north western corner of the Mahdouma valley and contains logs VA and VB. The marl member of section M-NW has been sampled for biostratigraphy, magnetostratigraphy and grain-size.

In contrast to the Jebel Haricha sections, the blue marl member is unconformably overlain by a mainly conglomeratic limestone sequence (**Fig. 13, a & b**).

The conglomeratic limestones showed fining upward sequences and mainly cross-lamination. The matrix consisted of bioclastic sediments which were often tube-shaped and carbonate coated. The clasts of the conglomerates mainly consisted of crystalline mudstones, rounded wacke-stones and carbonate concretions of algal-origin.

North of section M-NW, on the eastern side of the valley, log VN was constructed. Section M-NE consists of a 5 meter thick outcrop (**Fig. 13e**) with approximately 15 meters of visible lateral variations.

In contrast to section VB, the contact with the marls below was not visible. This section is composed of a finer grained conglomeratic sequence alternating with more sand rich intervals. Some of the beds showed channel features whereas others had a more wavy erosional surface. The dominant sedimentary

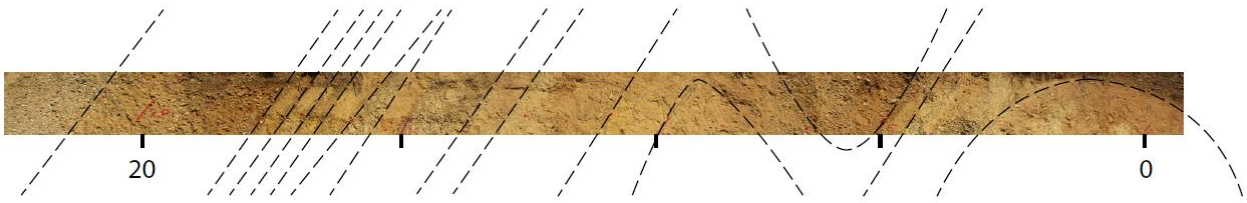

***Fig. 11** Panoramic picture of log HT with an interpretation of the folded bedding planes (black dashed lines).*

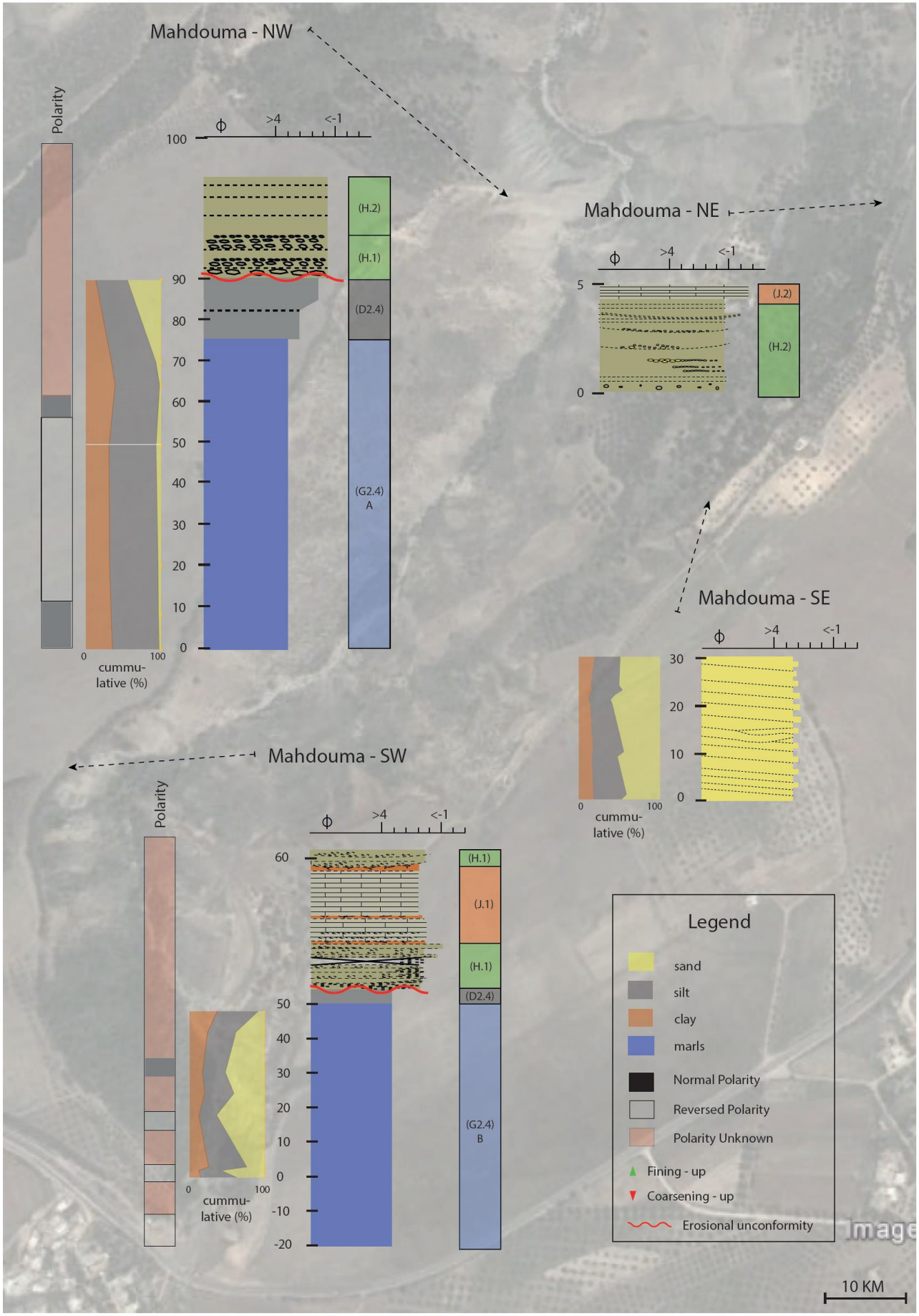
Mahdouma - NW
Polarity
ϕ
>4
<-1
100
90
80
70
60
50
40
30
20
10
0
(H.2)
(H.1)
(D2.4)
(G2.4)
A
0
100
cummu-
lative (%)
Mahdouma - NE
5
0
(J.2)
(H.2)
Mahdouma - SE
30
20
10
0
Mahdouma - SW
60
50
40
30
20
10
0
-10
-20
(J.1)
(G2.4)
B
Legend
sand
silt
clay
marls
Normal Polarity
Reversed Polarity
Polarity Unknown
Fining - up
Coarsening - up
Erosional unconformity
10 KM

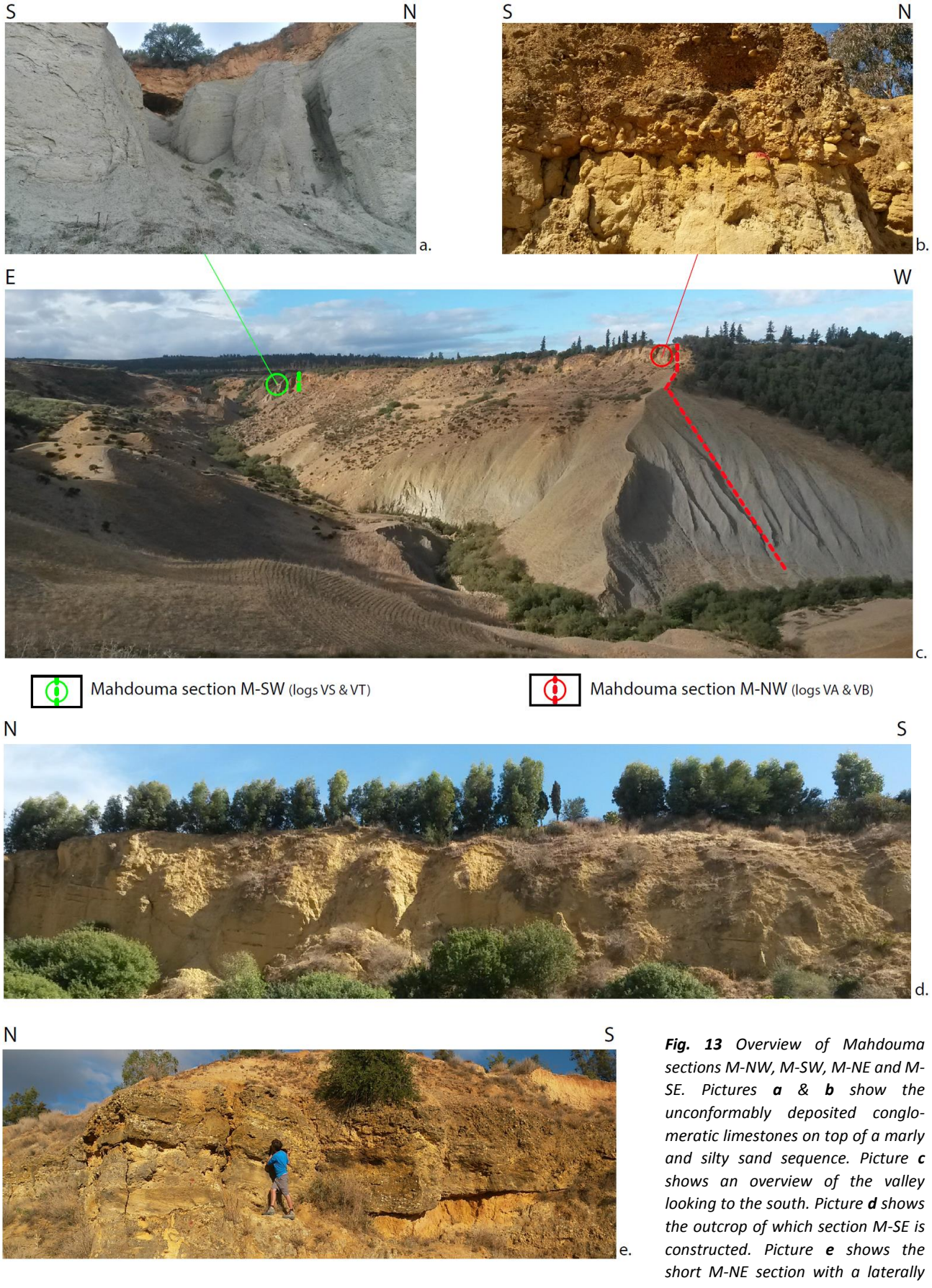

Fig. 13 *Overview of Mahdouma sections M-NW, M-SW, M-NE and M-SE. Pictures* ***a*** *&* ***b*** *show the unconformably deposited conglomeratic limestones on top of a marly and silty sand sequence. Picture* ***c*** *shows an overview of the valley looking to the south. Picture* ***d*** *shows the outcrop of which section M-SE is constructed. Picture* ***e*** *shows the short M-NE section with a laterally occurring palaeosoil (Menno for scale).*

structures were fining-upward sequences and cross-lamination. One of the most distinct features of this section was the lateral occurrence of a channel shaped orange colored palaeo-soil (**Fig. 13e**), and oncoidal grainstones in the upper part of the section of which the bedding was wedge shaped.

The conglomeratic limestone of section M-SW is the lateral equivalent of the top of section M-NW. The marls in this section have been sampled for magnetostratigraphy, biostratigraphy and grain-size. This section is located at the western flank in the south of the Mahdouma valley (**Fig. 13 a & c)** and is also unconformably overlain by conglomeratic limestones. The upper part of this section consists of a conglomeratic limestone with a bioclastic, carbonate coated matrix. The beds are predominantly channel shaped in the bottom part, with a fining upward Granule to cobble conglomeratic limestone. Towards the top, channel features disappear and finer conglomeratic packstones occur. Within this stratigraphic unit there are also signs of very reddish, thin palaeosoils interbedded with the conglomerates in the top of the section.

Section M-SE which has been studied in a different way compared to the other sections as explained above, consists of a yellowish – laterally extensive sandstone formation, located on the eastern flank of the Mahdouma valley in which up to approximately 4 meter thick fore-set like structures have been observed from a distance. A closer look revealed an apparent massive sandstone formation with less indications for these fore-sets. Bedding however has been noticed and measured. Since this formation is laterally extensive, is approximately 15 m high and has a low dipping angle, a different approach has been used. The section is laterally divided in 4 locations (location 1 furthest north – location 4 furthest south).

This section stratigraphically starts with apparently alternating beds of fine sand and sandy silts. Indications for bioturbation, erosional lamination and tiny shell remains have been found. The overall appearance of the outcrop showed a thickening well sorted and cross-laminated sequence. An estimated 10-20 m up in stratigraphy revealed channel shaped, through-cross bedded alternations of sandy and silty deposits. The through cross bedded channels contained orange coloured sand silt layers miced up with sandy, greyish and reddish laminations. Furthermore, reworked grey lenses of silt occurred in a more reddish matrix accompanied by bioturbation and sandy rip-up clasts up to 2cm in diameter. At an estimated height of 20 m an increase in the size and amount of shell remains (up to 5 cm) has been documented in an orange sand and grey more silty, thickening upward sequence.

Site M-NW (m)	Dip-direction	Palaeo-current direction
2	06 – 280 W	26 – 026 SW 17 – 050 SW
3	15 – 270 W	
M-NE (m)		
1		08 – 303 S 08 – 306 S
2	16 – 307 S	20 – 27 SW 20 – 041 N
3		10 – 042 N
4		19 – 160 SW

Site M-SE (location)	Dip-direction	Palaeo-current direction
1	10- 211 S	050 NE 060 NE 215 SW
3		100 E 120 E 130 SE

Table 2. *Dip- and palaeo-current directions results obtained from measurements in the Mahdouma valley.*

Further information regarding the results of the sedimentary logs in the Mahdouma section, such as dip-directions and palaeo-current directions can be found in **table 2.**

5.2. Grain size analyses

The results of the grain size analyses have been plotted with their stratigraphic height on the y-axis and varying parameters on the x-axis to image grain-size parameter variation throughout the stratigraphy of the sections (**Appendix 4**). In order to facilitate the ability to resemble the results of all the sections, multiple graphs have been constructed in which the grain-size results of all individual logs have been plotted (**Fig. 14**). For each graph, the standard deviation is plotted on the x-axis whereas variable parameters, consisting of the; graphic mean, skewness and kurtosis phi values are plotted on the y-axis. These graphs are a mere indication of the concistancy in grain-size parameters. The results are predominantly based on the stratigraphically plotted parameters.

Fig. 15 shows a graph containing all

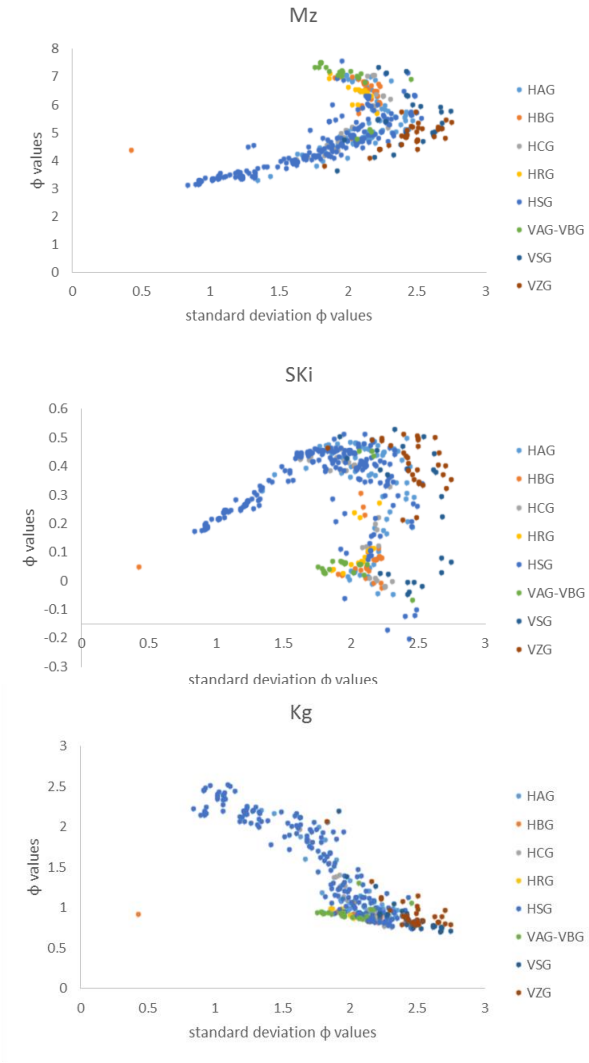

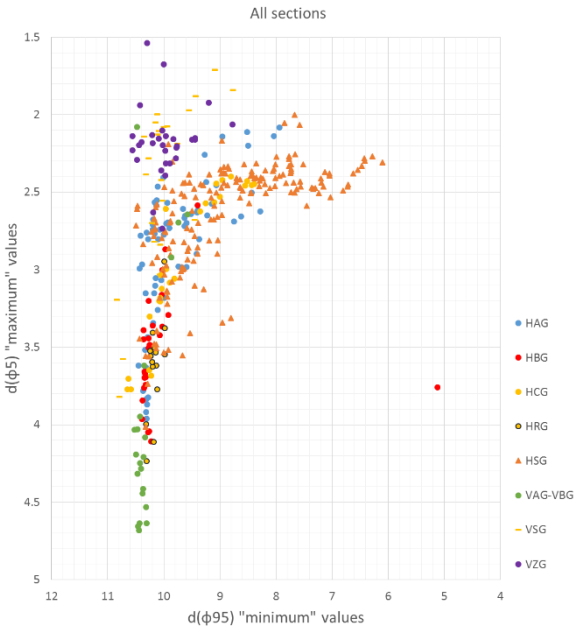

Fig. 15 *Graphs showing all results of the "tail" values of the distribution curve of all samples plotted for each log-location. The fine tail is plotted on the x-axis whereas the coarse tail is plotted on the y-axis.*

Fig. 14 *Graphs showing all results of the (top) Graphic mean, (middle) Skewness and (bottom) Kurtois values plotted against the standard deviation ϕ values.*

Note to both figures: legend is given in log names, names beginning with H correspond to JH and with V to Mahdouma.

distribution curve "tail" values. This graph mainly indicates that for logs HA (bottom of section JH-S) and HS (top of section JH-N) an increase in maximum grain-size values corresponds to an increase in minimum grain-size values as is to be expected.

Furthermore, in order to facilitate the verbal distinctions between fractions of clay, silt and sand in the samples, the slightly altered textural classification scheme for siliciclastic deposits by Shepard (1954) has been used. The results of these plots indicate that the samples for all sections are deposited within a certain cumulative range, as is marked in the figures (**Figs 16 – 20**).

- Section JH-S -

The grain-size results plotted in the ternary diagram (Shepard, 1954) (**Fig. 16**) show that section JH-S is made up of clayey-silt, sandy-silt, silty-sand and sand deposits. The clayey-silts dominantly belong to the blue marl member, however the complete spread is covered by the sandy deposits of logs HA and HC (bottom and top of section JH-S respectively).

The mean phi-values plotted against the stratigraphic height (**Appendix 4.1**) show a range of mean grain-sizes from fine silt to very fine- and fine-sand (See Wentworth scale for corresponding phi-values, **BOX 1).**

Furthermore, the results of the mean phi-values plotted against the stratigraphic height also show that the range of mean grain-sizes is at its maximum between 200 to 251 meters up in stratigraphy, indicating that the differences between mean-minimum and mean-maximum grain-sizes is largest. The range of mean grain-sizes in the blue marl member (±80 – 200 m) is smallest, except for the sample at 170 m which shows a peak of increased mean grain-sizes present in that sample. As a result, the graphs show that the relative range of grain-sizes between beds increases when ignoring the blue marl member. A fining trend exists from the bottom of the section

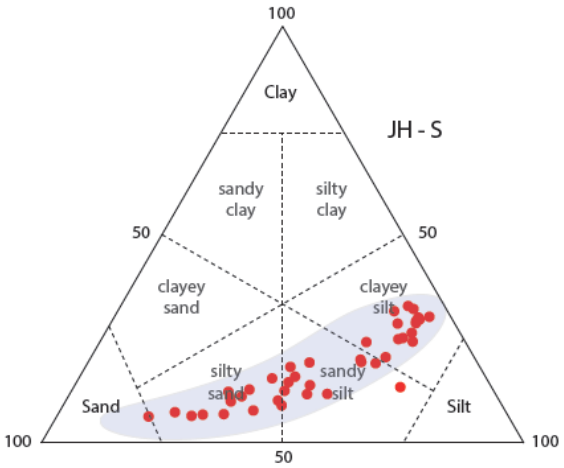

Fig. 16 *Ternary diagram of section JH-S (Shepard, 1954) showing the verbal cumulative composition of clay, silt and sand. The greyish area represents the range in which all of the different samples of all sections are located, indicating that all deposits belong to a similar grain-size related depositional environment.*

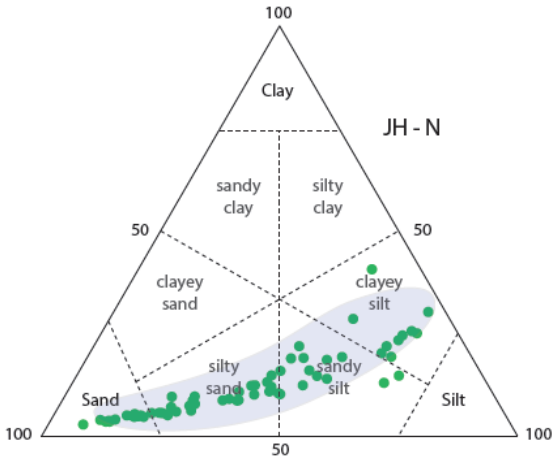

Fig. 17 *Ternary diagram of section JH-N (Shepard, 1954) showing the verbal cumulative composition of clay, silt and sand.*
NB; information regarding the greyish area, see Fig. 16.

towards the blue marl member and a coarsening trend from the blue marl member up-wards.

The standard deviation phi values range from 1.3 ϕ up to 2.5 ϕ (**Appendix 4.1**), indicating that the samples are poorly- to very poorly sorted. The graph shows a relative lack in trend changes, indicating that throughout the section no real differences in standard deviation occur.

The majority of the skewness values (**Appendix 4.1**) lie within a range of +0 and +0.45, indicating that the majority of the samples tends to be fine skewed. The skewness graph shows a trend similar to the graphic mean trend, where the coarser grained samples are more fine skewed than the samples with higher graphic mean ϕ values.

The samples of the blue marl member are all near symmetrically skewed with the exception of two samples that also strongly deviate from the trend in the graphic mean graph (110 m and 170 m). Furthermore the range of values is concentrated in the bottom part of the section (0 – 50 m) indicating that the samples are all fine- to strongly fine skewed, whereas the top part of the section (210 – 252 m) shows a broad range of symmetrically to strongly fine skewed samples.

The graphic kurtosis values increase when the sharpness or peakedness of a grain-size frequency curve increases. In the case for the JH-S section (**Appendix 4.1)** the sharpness is very moderate, except for some beds in the lower and upper part of the section, which show kurtosis values of >2, indicating sharp peaks which hence indicate better sorting in the central portion of the grain-size distribution than in their tails.

The graph of **Appendix 4.1.** shows the average 5th vs the average 95th percentile phi values determined from the cumulative curve (the "tales"). Hence giving an indication of the grain-size range for each sample. The "maximum" grain-sizes represent the 5th percentile phi values whereas the "minimum" grain-sizes represent the 95th percentile phi values. The results of the range of grain-sizes for section JH-S indicate that the difference in minimum and maximum grain-size values is lowest for log HB which is entirely made op of samples taken in the blue marl member. Largest grain-sizes occur in log HA which represents the bottom part of the section.

- Section JH-N -

The grain-size results plotted in the ternary diagram (Shepard, 1954) (**Fig. 17**) show that section JH-N is made up of clayey-silt, sandy-silt, silty-sand and sand deposits, similar to the results of section JH-S. The clayey-silts dominantly belong to the blue marl member, however the complete spread is covered by the sandy deposits of log HS (top of section JH-S). As discussed before, changes in the sandy sequence of section JH-N occur, and mainly comprise a decrease in silty beds towards the top. This change however can't be recognized in the ternary diagram, since both the lower as the upper sandy sequence cover the entire range of cumulative fractions.

The mean phi-values plotted against the

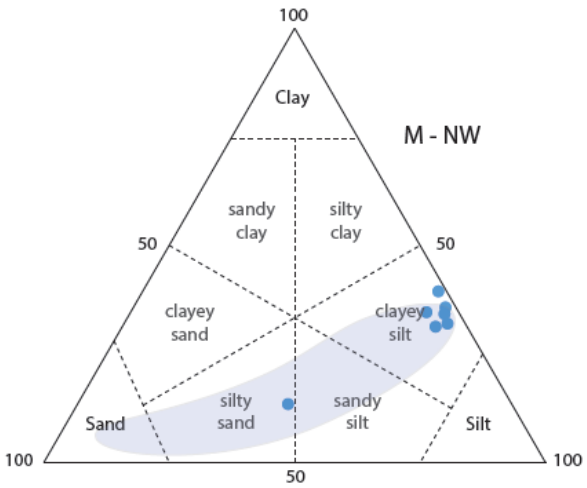

Fig. 18 *Ternary diagram of section M-NW (Shepard, 1954) showing the verbal cumulative composition of clay, silt and sand.*
NB; information regarding the greyish area, see Fig. 16.

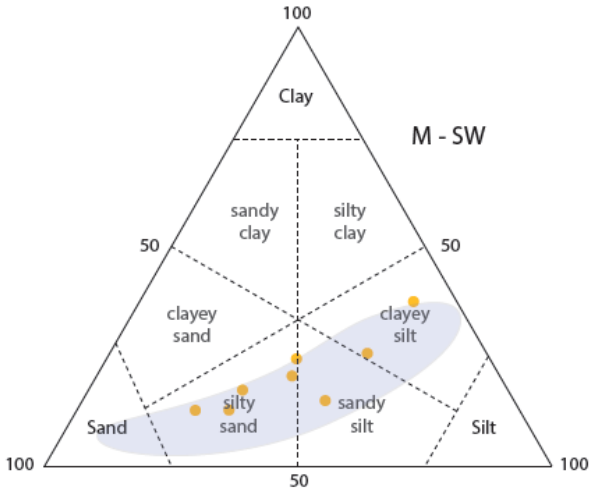

Fig. 19 *Ternary diagram of section M-SW (Shepard, 1954) showing the verbal cumulative composition of clay, silt and sand.*
NB; information regarding the greyish area, see Fig. 16.

stratigraphic height (**Appendix 4.2**) show a range of mean grain-sizes from very fine silt – fine sand. Furthermore, the results of the mean phi-values plotted against the stratigraphic height show that the range of mean grain-sizes is highest in the upper part of the section where sandstones are interbedded with siltstones, as well as beds that consist of both sand and silt. The range of mean grain-sizes in the blue marl member is smallest, as also indicated in the grain-size results of section JH-S. When ignoring the grain-sizes of the blue marl member, the range of mean grain-sizes is monotonous, but relatively high in the upper part of the section (140 – 320 m).

The standard deviation phi values are in the range of 0.8 and 2.6 (**Appendix 4.2**), indicating a verbal sorting range of well- to very poorly sorted sediments. A trend concerning the range of standard deviation values occurs, indicating that between samples there is a large range in the upper part of the section where sandstones and siltstones are intercalated, whereas the range in standard deviation is small in the blue marl member. The best sorting occurs in some of the coarsest samples of the upper part of section JH-N as can also be seen in the graph where the coarse tales are plotted versus the fine tales (**Appendix 4.2**).

The calculated skewness results (**Appendix 4.2**) show a wide range of values in the upper part of the section (log HS) with values ranging from -0.2 to +0.5. These results indicate a range from coarse skewed to strongly fine skewed samples. On average the blue marl member shows lower skewness values, indicating more symmetrically skewed samples than the intercalated sandy part of the section.

The graphic kurtosis values increase when the sharpness or peakedness of a grain-size frequency curve increases. As is the case for the skewness (**Appendix 4.2**), a large amount of spread occurs in the upper part of the JH-N section, indicating large varieties of kurtosis in close proximity. Nevertheless, on average, the upper part of the section with increased sand content shows better sorting in the central portion of the grain-size distribution compared to the tales.

The graph showing the tales of the grain-size distribution curve indicates that the minimum grain-size is drastically lower in the upper part of the JH-N section, where the amount of siltstones decreases to near zero, also indicating that the range of grain-sizes decreases and hence better sorting occurs. The minimum grain-sizes for the blue marl member is constant, whereas the maximum grain-sizes vary.

- Section M-NW -

The grain-size results plotted in the ternary diagram (Shepard, 1954) (**Fig. 18**) show that section M-NW is made up of mainly clayey-silt and one sample, the upper-most sample at 90 m stratigraphic height corresponds to a verbal cumulative fraction of silty-sand. The results for section M-NW are deposited in the same range as indicated for the results of sections JH-S and JH-N.

The mean phi values for section M-NW clearly show a coarsening up-ward trend (**Appendix 4.3**). The mean grain-size changes from very fine silt in the blue marl member towards coarse silt 3 m below the erosional unconformity (log VB). Due to the lack of sandstones in this formation, the deviation of mean grain-sizes is nearly lacking.

The standard deviation phi values measured in section M-NW **(Appendix 4.3)** show a slight decreasing upward trend. The range of standard deviation phi values lies between +1.55 and +2.5 which compares to a verbal sorting of poorly- to very poorly-sorted sediments.

The results of the skewness phi values (**Appendix 4.3)** indicate a sudden increase in skewness values near the erosive contact with the conglomerates at 90 meters of stratigraphic thickness. Throughout the blue marl member the skewness values indicate a near symmetrical skewness distribution whereas the uppermost sample in this section is very strongly fine skewed indicating only a minor amount of coarser sediment in the tales.

The graphic kurtosis values of section M-NW (**Appendix 4.3**) show an increase towards the stratigraphic top. Despite the increase in ϕ values, the samples in this section show only a small peak in the central portion of the grain-size distribution compared to the tails of this distribution curve.

The graph showing the tales of the grain-size distribution curve indicates that the minimum grain-size is constant throughout the M-NW section, whereas the maximum grain-sizes vary.

- Section M-SW -

The grain-size results plotted in the ternary diagram (Shepard, 1954) (**Fig. 19**) show that section M-SW is made up of clayey-silt, sandy-silt and silty-sand. The results for section M-SW are deposited in the same range as indicated for the results of all previously discussed sections. By comparing the cumulative graph of **Fig. 12**, the location of each sample can be obtained. The dominant trend however is an up-ward decrease in the fraction of sand.

Section M-SW is located at the south eastern flank of the Mahdouma valley (**Fig. 6**) starting in what appeared to be the blue marl member and ending with with unconformably deposited conglomeratic limestones.

The mean ϕ values of section M-SW are broad ranged in the bottom and more concentrated towards the top. The mean ϕ grain-size decreases from an average of 5 (coarse silt) at the bottom to 7.5 (fine silt) at the top, which is comparable to the results of section M-NW in reversed order.

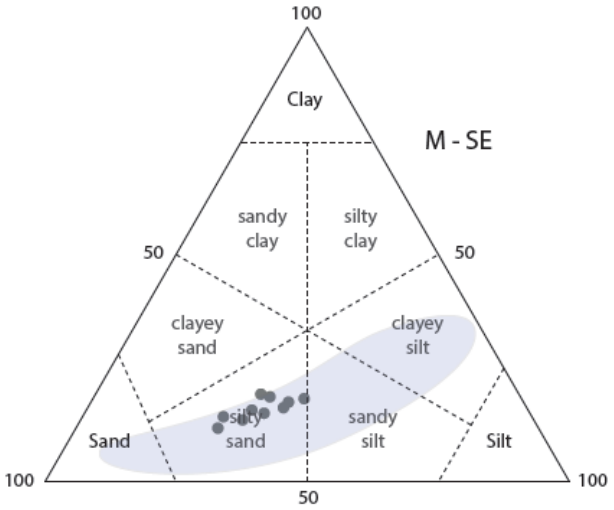

Fig. 20 *Ternary diagram of section M-SE (Shepard, 1954) showing the verbal cumulative composition of clay, silt and sand.*
NB; information regarding the greyish area, see Fig. 16.

The standard deviation phi values (**Appendix 4.4**) indicate that the sediments are very poorly sorted. The range of values at 17 m however is large indicating a deviation in measured results of the same sample.

The skewness results obtained from the samples of section M-NW are slightly alternating between near symmetrically- and strongly fine-skewed, indicating that the samples tend to an excess in fine particles.

Kurtosis ϕ values are near constant for this section, indicating that the sharpness of the grain-size frequency curve remain more or less the same. These values show a low peak, which means that the sorting in grain-size distribution is well distributed from the center to the tails.

- Section M-SE -

The grain-size results plotted in the ternary diagram (Shepard, 1954) (**Fig. 20**) show that section M-SE is made up of silty-sand. The results for section M-SE are deposited in the same range as indicated for the results of all previously discussed sections as well.

Since this formation is laterally extensive (**Fig. 13 d**), is approximately 15 m high and has a low dipping angle, a different approach has been used. The section is laterally divided in 4 locations (location 1 furthest north – location 4 furthest

south) from which multiple grain-size samples have been taken. Hence, grain-size graphs use an estimated stratigraphic height based on changes in lateral location. No clear trends in ϕ values can be observed from the graphs of section M-SE (**Appendix 4.5**). The mean grain-size average indicates values that compare with coarse silts, which in turn is comparable with the sandstone deposits of the Jebel Haricha sections as well as section M-SW.

The standard deviation indicates very poorly sorted sediments without a real variation throughout the stratigraphy of this section, the mean standard deviation values however are relatively high compared to the mean values of other sections.

Resulting ϕ values for skewness show that the sediments are strongly fine skewed, indicating that there is a large excess of fine particles in the "tails".

The resulting kurtosis ϕ values indicate low peakedness of the sorting in the central portion of the grain-size distribution compared to the tails.

The distribution curve (**Appendix 4.**5) indicate that the coarsest sediments can be found in section M-SE, with values corresponding to medium sand. The majority of the samples however range from 10 to 2.2 ϕ which corresponds to clay and fine sand respectively.

5.3. Thinsections

Thinsections are used in sedimentary petrology to investigate the optical properties of the minerals present. Mineral composition and textural features of the thin-sections are based on the optical properties of the minerals present in the thin-section and can help to reveal the origin and evolution of the parent rock.

Since I lack a background in thin-section petrology, multiple online sources were used to generally classify the samples *(e.g. Imperial College Rock Library)*.

In total, 19 samples were collected during the fieldtrip of which 8 have been used for optical-petrology. The analysed thin-sections all belong to the Jebel Haricha sections and are spread stratigraphically over the entire formation (**fig. 9**). The thin-sections belong to the sandstones, since microscopy of finer grained rock was nearly impossible.

The thin-section analyses was mainly based on; 2-dimensional sphericity, angularity, sedimentary features, porosity, matrix and mineralogy using classification schemes depicted by *Tucker (2001)*. Percentage estimations were achieved by percentage estimation comparison charts (Folk et al., 1970).

- *Morphological description* –

The general resultant morphological descriptions of the thin-sections (**appendix 5**) indicate high lithic content, dominantly composed of chert grains. Furthermore, the samples contain 25 – 40 % quartz, showing moderate sphericity and sub-angular to sub-rounded angularities. All thin-sections contain mica content in the form of biotite, muscovite or glauconite and contain opaque and heavy minerals.

The stratigraphically lowermost sample (log HA, 1.3 m – section JH-S) consists of low to high 2D spheric, angular to sub-rounded clasts. It contains bioclastic material, is dominantly grain supported and has very low porosity. The mineralogical composition consists of 30% quartzose grains, 3% micas, 30% lithic – dominantly wacke fragments, 20% matrix and contains 5 – 10 % of calcite. Based on the sandstone classification of *Pettijon et al. (1987)*, this sample is classified as a lithic wacke.

Sample HA 61 (section JH-S log HA) contains medium spheric, sub-rounded to rounded clasts. The sample is irregularly laminated (not oriented) and has a matrix supported fabric. Shell remains and bioclastic fragments have been observed, as well as fluid inclusions in approximately 2% of the grains. The sample has a very low porosity (<1%) and 10 – 20 % matrix consisting of very fine, brownish grains and calcite. The mineralogical composition consists of 25% quartzose grains, 2% of feldspar in the form of plagioclase, 2% of heavy minerals, 5% amphibole – indicating immature sediments and 30 – 40 % of (chert) lithic fragments. This sandstone sample is classified as an immature lithic wacke or a litharenite.

At 205 m stratigraphic height in section JH-S, sample HB 65 (log HB) was taken at the transition from the blue marl member to the turbeditic sand/silt alternations of log HC. The thin-section of this sample shows medium to high spheric and sub-rounded clast. Small iron concretions were observed at the bottom of this thinly laminated and a dominantly grain supported sample. The sample contained 5% porosity and

approximately 30% of matrix. The sample consists of 35% quartz, 10% feldspar (plagioclase), <5% calcite, 2% heavy minerals, 3% halite and 15% of lithic, most likely chert fragments. Classification of this sandstone results in a lithic to feldspatic wacke.

At 269 m stratigraphic height in section JH-N (log HS, 127m) the sample shows low to high spheric, sub-angular clasts in a grain supported fabric. The sample has very low porosity and approximately 15% matrix with occasionally bioclastic content. The mineralogy of the sample consists of 30% quartz, 5 – 10 % calcite, 3% micas (glauconite and muscovite) and 35% of lithic clasts. Classification of this sandstone results in a litharenite or lithic wacke.

At 274 m stratigraphic height in section JH-N (log HS, 131m) the sample has medium spheric, sub-angular to sub-rounded clasts with small iron nodules at the bottom. The percentage of matrix and porosity increases up-ward in this thinly laminated dominantly matrix supported sample. Porosity ranges from 10 – 35 % whereas the matrix is 35%. The mineralogy of the sample consists of 30 quartz, 5% feldspar (albite and plagioclase, where albite indicates immature sediments), 1% micas, 2% heavy minerals and 20% of lithic fragments. This sample furthermore contained 5% of unidentified, brownish minerals with a moderate to high relief. Classification of this sandstone results in a lithic wacke.

Thin-section sample HS 145, located at a stratigraphic height of 287 m in section JH-N contains medium to high spheric, sub-angular to rounded clasts. He sample shows a grain supported fabric with point contacts and a porosity of <5%. The sample contains approximately 15% matrix and a mineralogy of: 30% quartz, 6% Feldspar (orthoclase and plagioclase), 4% micas (biotite and muscovite), 1% heavy minerals and 25% lithic fragments. The classification of this sandstone can be a litharenite or a lithic greywacke.

The uppermost thin-section sample, sample HS 145.3, located at a stratigraphic height of 287.3 m in section JH-N contains low to high spheric, sub-rounded grains. The clasts in the sample gradationally become more rounded towards the top. Bioclast, very elongated angular clasts and lots of darker clasts under normal light have been observed. The porosity and matrix (5%) percentages in this sample are very low. The mineralogy of this sample shows a concentration of; 40% quartz, 5% halite, 5% heavy minerals, 1% micas (muscovite and biotite), 1% albite (hinting towards a low maturity sediment), 1% calcite and 40% of lithic fragments. This sample is classified as a litharenite.

Striking observations of the optical properties of the samples include: a low feldspar, high lithic content, an abundance of lithic wackes dominantly in the lower part of the complete section (JH-S and the start of the sand interval of section JH-N) and the occurrence of halite in the upper-most sand dominated part of section JH-N.

Wackes are generally associated with the deposition of turbidity currents in basins of various types, usually off continental margins, in back-and fore-arc basins *(Tucker, 2001)*. The immature composition of litharenites implies high rates of sediment production from supracrustal sources followed by short to moderate transport distances. Litharenites are usually associated with fluvial and deltaic settings, but lithic sandstones are also common in the Alpine Molasse Basin, a foreland basin formed by thrust loading after continental collision *(Tucker, 2001)*.

5.4. Magnetostratigraphy

During the fieldwork 37 palaeomagnetic cores have been collected to determine the polarity and age of the marly intervals. Samples have been taken in and in close proximity to the "blue marl member" in sections JH-S, JH-N, M-NW and M-SW. The quality of the results varies due to recent overprint of the magnetic signal, however the marly intervals generally show good results.

The results of the magnetostratigraphic analyses will be separated based on locality. The results of the Jebel Haricha sections will be given first, after which the results of the Madhouma sections will be explained. The results of the declination and inclination can be found in **Appendix 6**. and 3 Zijderveld diagrams (**Fig. 21**) are added to show examples of the temperature controlled demagnetization steps. Furthermore the degree of rotation, indicative for the rotation of the study area and useful for back-rotating the palaeo-current directions will be explained.

- Jebel Haricha -

The 25 magnetostratigraphic samples of the Jebel Haricha sections mainly consists of samples taken from the blue marl member. Several cores however (section JH-S) have been

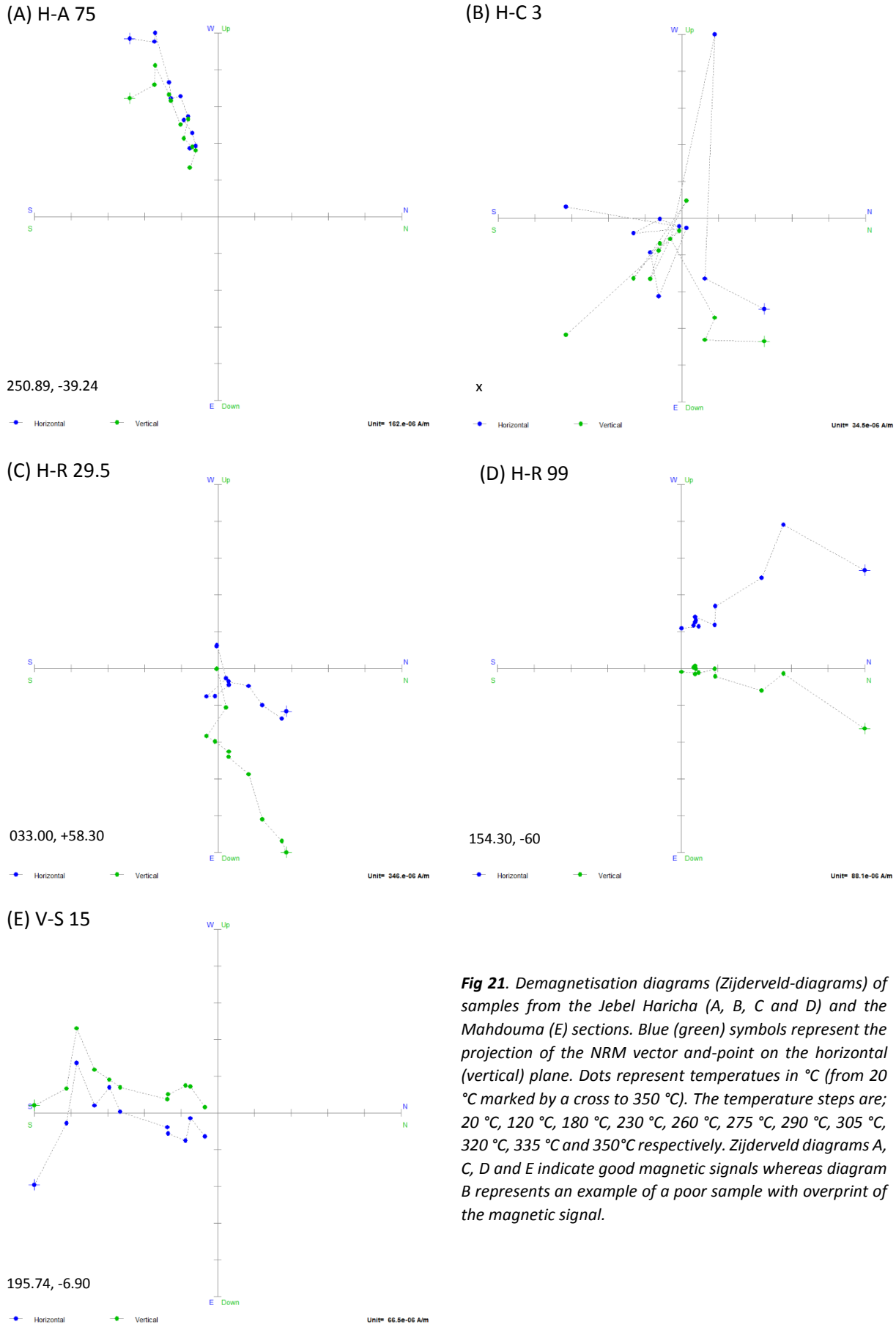

***Fig 21**. Demagnetisation diagrams (Zijderveld-diagrams) of samples from the Jebel Haricha (A, B, C and D) and the Mahdouma (E) sections. Blue (green) symbols represent the projection of the NRM vector and-point on the horizontal (vertical) plane. Dots represent temperatues in °C (from 20 °C marked by a cross to 350 °C). The temperature steps are; 20 °C, 120 °C, 180 °C, 230 °C, 260 °C, 275 °C, 290 °C, 305 °C, 320 °C, 335 °C and 350°C respectively. Zijderveld diagrams A, C, D and E indicate good magnetic signals whereas diagram B represents an example of a poor sample with overprint of the magnetic signal.*

taken in the siltstones that are intercalated with sandstones (turbidites) above (log H-C) the blue marl member. Both blue marl members (section JH-S and JH-N) in the Jebel Haricha area are expected to be equivalent since the lateral distance only spans 2km and hence are treated like-wise.

The magnetostratigraphic results are shown in **Fig. 9 & Appendix 6**, where small open dots indicate the results for temperatures of 290°C to 350 °C with steps of 15°C. The significance of the samples was based on Zijdeveld diagrams (**Fig. 21**). The declination and inclination vectors of significant samples with good signal results are plotted in the colored squares connected with black dotted lines.

The average magnetic signal components for the Jebel Haricha area indicate a declination of 250.7° and an inclination of -31.8° (**Appendix 6**). The rotation can be determined by subtracting 180° from the inclination, resulting in a clockwise rotation of 70.7°. Since dip-directions of the bedding in the Jebel Haricha area is consistent, it can be stated that rotation occurred post-depositional. In order to back-rotate palaeo-current directions an anti-clockwise rotation of 70° should be implemented.

Comparison of both blue marl members of the JH-S and JH-N section proves impracticable since the majority of the samples in section JH-N seems overprinted by post depositional magnetic signals. Most-likely were the samples of section JH-N contaminated by weathering. The results of H-R 1 however proves to be comparable with the results of section JH-S.

The magnetostratigraphic results for the Jebel Haricha section indicate that the blue marl member was entirely deposited during a period of reversed polarity. The lack of reversals in this member indicate that the deposition period of the blue marl member was relatively short. In order to make assumptions about the period, age and sedimentation rate in the blue marl member, results of magnetostratigraphy have to be compared to the biostratigraphic results.

- Mahdouma -

The 11 magnetostratigraphic samples of the Mahdouma section consists of samples taken from the marly intervals. Both marly sequences (section M-NW and M-SW) in the Mahdouma area are expected to be stratigraphically related since the lateral distance only spans 750 m. The dip direction of the bedding however is inclined towards the south indicating a stratigraphic offset with stratigraphically younger sediments towards that direction. Since the marly interval is horizontally eroded by a peneplainar erosional surface, older marl deposits are in contact with that unconformity in section M-NW compared to section M-SW.

The magnetostratigraphic results are shown in **Appendix 6 & Fig. 12**, where small open dots indicate the results for temperatures of 290°C to 350 °C with temperature steps of 15°C. The significance of the samples was based on Zijdeveld diagrams (**fig. 21**). The declination and inclination vectors of significant samples with good signal results are plotted in the colored, tilted squares.

Palaeo-magnetic results for the Mah-douma area can be divided in relatively good signals that indicate a reversed polarity at time of deposition, and signals that have a component of overprint and hence are relatively poor. The samples with a component of overprint generally also indicate, or hint to, deposition during reversed polarity. It is striking however that at stratighrapically increased height, the signal shows signs of normal polarity for both section M-NW and M-SW.

The average magneto-stratigraphic com-ponent for the marly member in both study-areas is equivalent. Declination and inclination results show a minor deviation, as can also be said for the difference in rotation. Further comparison of both area's however remains difficult since biostratigraphic samples for the Mahdouma section have not yet been examined.

5.5. Biostratigraphy

As stated before, the bio-stratigraphic results were obtained by *M.A. Tulbure*. The results come from a limited number of samples taken in both Jebel Haricha sections. The interpretation of age, depositional-environments and bathymetry are therefore preliminary. The results are divided in two categories, the results from the planktonic foraminifera and the results of the benthonic foraminifera.

- Planktonic foraminifera –

The *Gl. miotumida* group (**Fig. 9**) is continuously present throughout all the marly intervals of both Jebel Haricha sections, but its

abundance varies. At the bottom of section JH-S, the *Gl. miotumida* occurs in traces, after which it becomes common at a stratigraphic height of 44 m. At the base of section JH-N, *Gl. miotumida* occur in abundance, whereas it is common at a stratigraphic height of 140 m, at the beginning of the sandy interval.

The presence of the *Gl. miotumida* group (whose first regular occurrence is at 7.24 Ma) throughout the entire section indicates that the sedimentary succession belongs to the Messinian stage.

Neogloboquadrinids coiling direction is dominantly sinistral (sinistrally coiled), but a high number of dextrally coiled was found too. This pattern of sinistral to dextral oscillations was previously described by Sierro et al., 1993 and is common for assemblages of the Guadalquivir basin. Usually it occurs prior to event PF5 ***(Sierro et al., 1993)***, which is characterized by a sharp decrease in the *miotumida* group.

The presence of *Gl. scitula* is very rare or absent throughout both sections JH-S and JH-N. The few specimen found showed both dextral and sinistral coiling direction.

The overall biostratigraphic assemblage of the Jebel Haricha sections indicate that the sediments are of Early Messinian age. The *neogloboquadrinids* sinistral coiling direction suggests that the sedimentation at Jebel Haricha occurs before the change of coiling pattern PF5, dated at 6.29 in the Atlantic sections (see Sierro et al., 1993). Regarding the maximum age of the section, we refer to the Ain el Beida section in the adjacent Gharb-Basin *(Krijgsman et al 2004)*, where between cycles AEB6 and AEB 9 dextral and sinistral *neogloboquadrinids*, *G. scitula* dominantly sinistral and *G. miotumida* occured. The age of this interval, based on the astronomical tuning showed in *Krijgsman et al. (2004)*, is between cycles AEB 6 and AEB 9 - approximately 6.37 and 6.29 Ma.

- Benthonic foraminifera -

The benthonic foraminifera assemblage from the Jebel Haricha sections is composed by deep-water species (*Oridorsalis stellatus, Cibicides kullenbergi, Eggerella bradyi, Cibicides wuellerstorfi, Uvigerina peregrina, Valvuneria complanata, Cassidulina spid, Globobulimina*). The presence of deeper infaunal *Nonion bethealum*, which were only found in the upper part of section JH-N, indicate a trend of increasing bathymetry in the Jebel Haricha succession.

This benthonic foraminifera assemblage is characteristic of upper slope deposits (300 – 500 m) with a possible increase in bathymetry at the base of the sandy interval of section JH-N.

6. INTERPRETATION AND DISCUSSION

6.1 Facies description and interpretation

The facies description is based on the classification of deep sea sediments described by *Stow et al. (1986) (modified after Mutti & Ricci Lucchi, 1972)*. The facies classes are distinguished on the basis of grain-size internal organization and composition (Facies Classes A – G). Facies groups are distinguished on the basis of internal organization, structures and textures. Individual facies sub-groups are based on internal structures, bed thickness and composition.

The facies are assigned to stratigraphic units with comparable characteristics and trends. A facies diagram is constructed showing the main characteristics for each facies (Jebel haricha **Fig. 9 &** Mahdouma **Fig. 12**). The individual facies recognized are assigned to a palaeo-environment that is able to explain the stratigraphic characteristics of that facies.

- Jebel Haricha –

CLASS C

Facies assigned to class C consist of sand – mud units with varying differences in the fractions of sand and silt (**Fig. 9**). Since the majority of deposits belonging to this facies class are organized structures, the stratigraphic units assigned to this class are sub-grouped as organized facies (C2). This facies class is dominantly composed of alternating sand rich beds with a thin- to medium-bed thicknesses and silt – clay rich medium- to very thick-bed thicknesses.

Further facies sub-divisions are based mainly on internal bed features and include both facies C2.1 and Facies C2.2. Both facies are characterized mainly by a variety of: cross- and parallel-lamination of which the latter is also found in the silty layers, it should be noted however that the majority of beds showed no or un-clear sedimentary features. Furthermore, erosional surfaces were recognized of which the major features were composed of scour-marks. Other distinct features of this facies group include

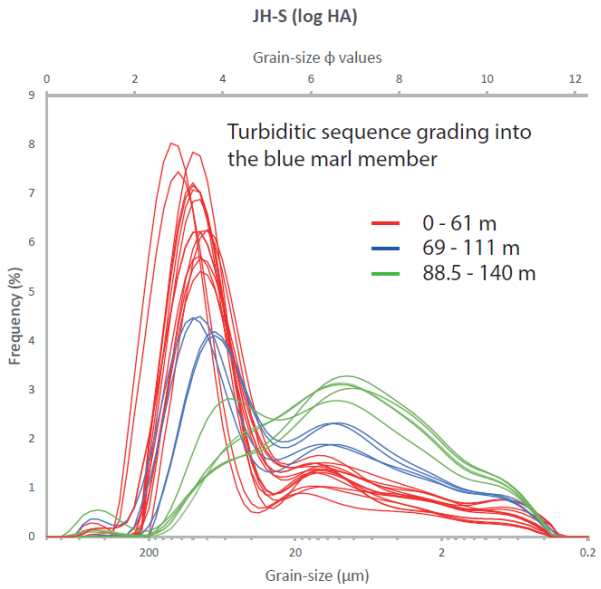

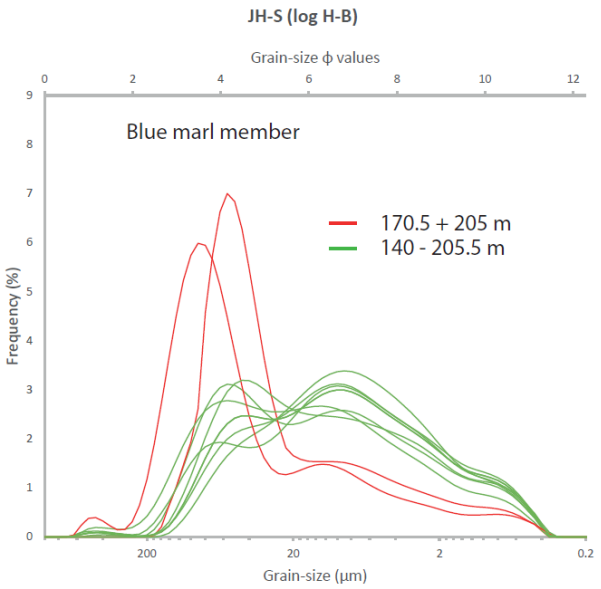

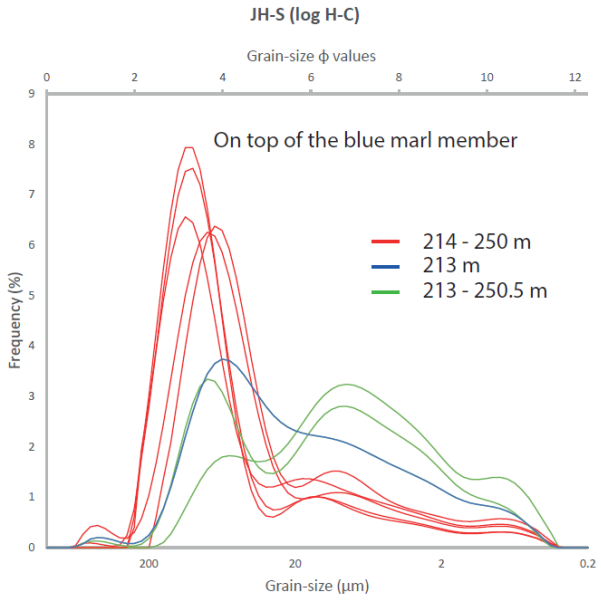

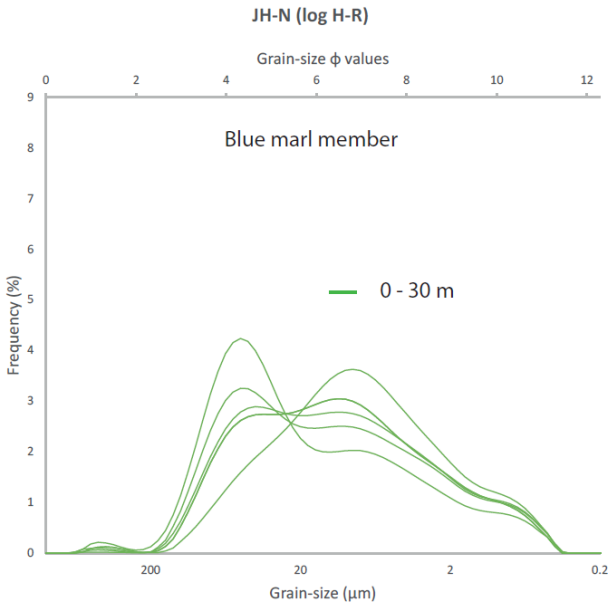

iron crusts occurring both at tops and bottoms of sand rich beds, as well as varying secondary manganese concretions. The stratigraphic units of this facies class showed mainly moderately bioturbated sediments (main species: Rhyzocorralium) and varying amounts of pectinidae and other bivalvia.

The thinsection related to facies C2.1 (H-B 65) indicated medium to highly spheric sub-rounded clasts with thinly laminated iron concretions. The sample has been classified as a lithic- to feldspatic-greywacke. The thinsections related to facies C2.2 (H-A 1.3 & H-A 61) indicated medium- to highly-spheric sub-rounded clasts and are classified as immature greywackes or litharenites. Wackes are generally associated with the deposition of turbidity currents in basins of various types, usually off continental margins, in back-and fore-arc basins *(Tucker, 2001)*. The immature composition of litharenites implies high rates of sediment production from supracrustal sources followed by short to moderate transport distances. Litharenites are usually associated with fluvial and deltaic settings, but lithic sandstones are also common in the Alpine Molasse Basin, a foreland basin formed by thrust loading after continental collision *(Tucker, 2001)*.

Both facies C2.1 and C2.2 are distinguished by their stratigraphic change in bedding alternation. Facies sub-group C2.1 is composed of a stratigraphic decrease in silt interval bed-thicknesses with stratigraphically increasing amounts of sand rich deposits, whereas the dominantly occurring facies sub-group C2.2 is characterized by a stratigraphical increasing amount of silt intervals and bed-thicknesses. Facies sub-group C2.2 is furthermore characterized by a stratigraphic decrease in sand

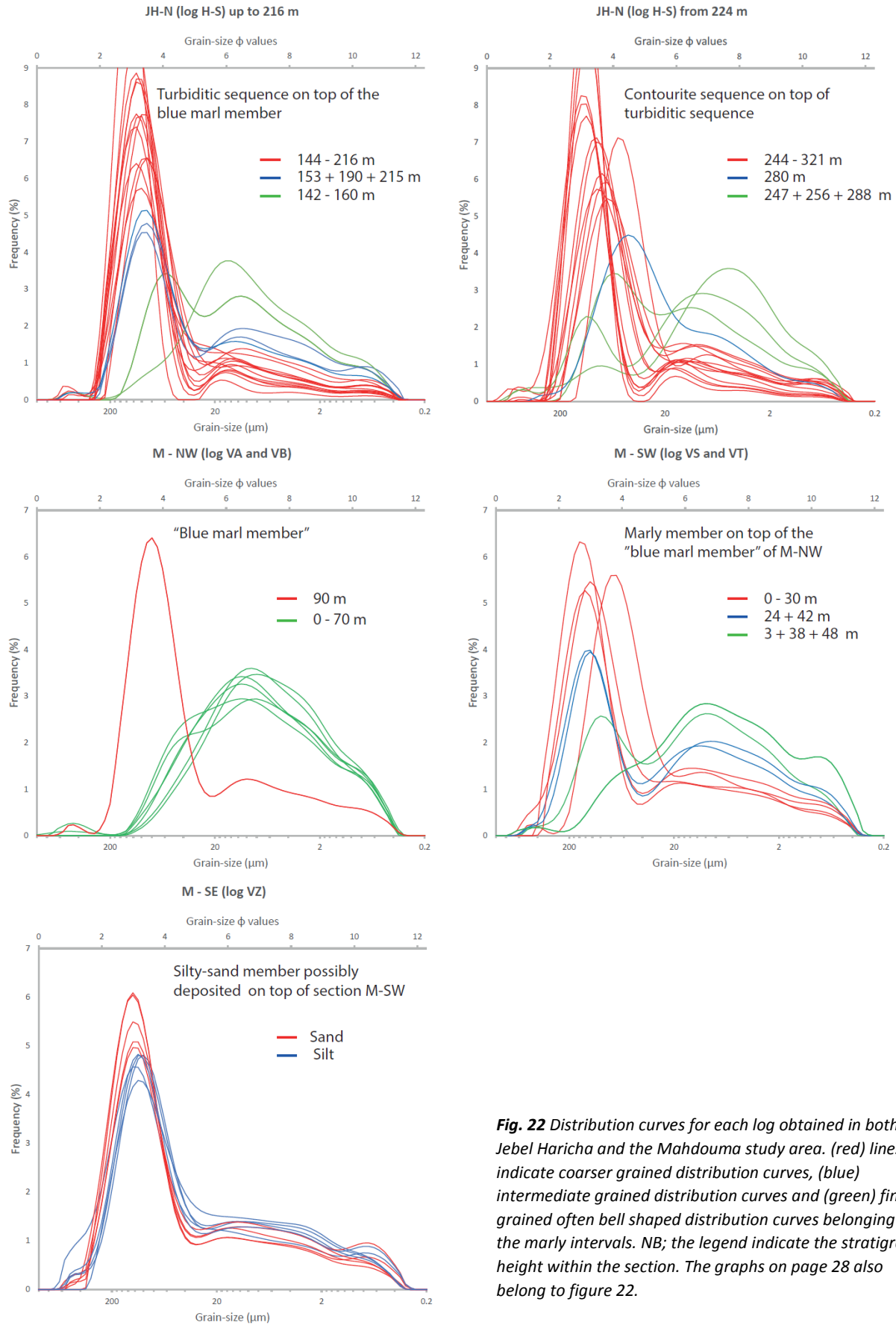

Fig. 22 *Distribution curves for each log obtained in both the Jebel Haricha and the Mahdouma study area. (red) lines indicate coarser grained distribution curves, (blue) intermediate grained distribution curves and (green) finer grained often bell shaped distribution curves belonging to the marly intervals. NB; the legend indicate the stratigraphic height within the section. The graphs on page 28 also belong to figure 22.*

rich deposits.

Facies C2.1 is recognized at transitional sites where very fine clayey silt depositsional sequences show a stratigraphic change towards coarser grained depositional environment. These transitional sites occur both at the upper-most

location of the blue marl members (facies G2.4) of both section JH – S and JH – N. Another transitional sequence belonging to facies C2.1 occurs as a transition from clayey silts to sandy silts at 240 m stratigraphic height in section JH – N.

Facies C2.2, the dominant facies in both Jebel Haricha sections occurs both below and above the blue marl member, separated by thin transitional sequences (above – C2.1 and below – D2.4).

The findings of this work are similar to the findings denoted in the *ERICO report of (1991)*, in a sense that this sedimentary unit (Facies C2) belongs to a turbiditic sequence. The large amount of clayey silt- and silt intervals indicate middle- to distal ramp-settings with high density turbiditic currents *(Reading et al., 1996)*. The major differences between both facies sub-groups show changes in both increasingly turbiditic current influenced environments (C2.1) and decreasingly turbiditic influenced depositional environments (C2.2).

The structureless mainly sandy beds interbedded in this turbiditic sequence are hard to interpret. They however, are said to be common in deep-water successions, often interbedded with normal turbidites *(Reading et a., 1996). Stow, Brackenburg and Johansson (1994)* concluded that these massive sands were most commonly deposited by: freezing of sandy debris flows; collapse fallout from; or continuous aggradation beneath a high-density turbidity current (cited from: Reading, 1996). This however does not alter the palaeo-environmental interpretation.

Increases in grain size, and thus changes in turbidite grain-size distribution are directly related to increases in slope gradient *(Reading & Richards, 1994)*. Biostratigraphic results indicated a stratigraphic increase in palaeo-bathymetry resulting in a positive effect on accommodation space in the basin. It is generally accepted that this increase in palaeo-bathymetry resulted from subsidence of the basin. Subsidence could have been responsible for an increase in slope, triggering turbiditic currents and subsequently form turbidite deposits. Changes in the rate of subsidence could, in this case, be responsible for changes in depositional sequences (C2.1 vs. C2.2).

The onset of turbidite deposition is engendered by the subsidence phase which post-dates the Nappe emplacement. Subsidence is created due to flexure of the lithosphere caused by the Nappe emplacement itself. The depocenter of flexural subsidence is estimated to be 10 km or 10 km south of Sidi Kacem.

Reading et al. (1996) state that accommodation space in deep water is not generally an important depositional factor in deep-water clastic systems. Accommodation space in the source area however, particularly at the coast and shelf, is critical because it controls the extent of storage, bypassing and erosion and therefore supply to deep-water environments.

The statement of *Reading et al. (1996)* therefore favours a change in the accommodation space of the source area to be responsible for the deposition and the type of depositional sequences of the turbiditic unit deposited in the Jebel Haricha section. changes in accommodation space of the source area are most likely related to compressive tectonics in the mountain front. Therefore indicating that changes in the compressive regime could have occurred during the time of deposition.

CLASS D

The stratigraphic unit described to class D consist of silts and silt – mud units. This facies class exists of organized groups in the JH – S section and a disorganized group in the JH – N section. This facies class is dominantly composed of a thick (~ up to 15 m) mainly clay – silt sized sequence. Within the JH – S section this silty sequence is organized and composed of medium to thick beds with only minor thin, coarser grained beds (D2). In the JH – N section, the sequence is composed of a poorly exposed unorganized apparently massive siltstone (D1).

The facies groups in the JH – S section are sub-divided as an alternation of fining upward deposits (D2.4), whereas the facies groups in the JH – N section is sub-divided as a more or less massive silt deposit with unorganized or rather invisible alternations of grain-sizes (D1.2). Despite the fact that these deposits have been recognized as silt deposits, mainly facies D2.4 contains a rather high (~20%) lithic content.

Since facies D2.4 occurs within the turbidite facies (C2.2) it is proposed that depositional environments have not changed drastically, hence suggesting that the facies change is related to a change in sediment supply or tectonically controlled basin activity. The latter is also the case for facies D1.2, which consists of a higher silt fraction, indicating a more subtle environment or changes in sediment supply (see

class C).

Grain-size results obtained from the distribution curves (**Fig. 22**) indicate that the majority of the samples in facies class D are aligned between the average results of both sand beds and silt – clay beds (blue lines). Their relatively large grain-sizes indicate that pelagic or hemipelagic -sedimentation could not have solely been responsible for the formation of these deposits. The grain-size results furthermore indicate that the internal composition of the beds was not as well organized as expected during field observations.

Grain-size characteristics of fine-grained turbidies *(Kranck, 1984)* closely resemble both grain-size distribution and grain-size frequency curves obtained in this study (**Fig. 22)** The grain-size distribution curve indicates fine skewed distributions with relatively low Kurtosis. Fine-grained turbidite deposits result from low-concentration flows transporting mainly silt- and clay-sized material *(e.g. Kelts & Arthur, 1981)*. These low concentration turbidites or possibly hematurbidites are generally the result of increases in buoyancy after sediment fallout (Sparks, Bonnecaze et al., 1993), indicating a possibly more distal turbidite facies or late stage of turbidite deposition.

CLASS G

The stratigraphically thickest facies sequence is composed of the blue marls ("Marnes de Salé"). This stratigraphic unit is assigned to class G which describes low energy, fine grained, deep-water settings. The main group of class G consists of pelagic and hemipelagic sediments. Due to weathering, distinct beds and stratigraphic alternations were not recognized.

Since this stratigraphic unit is composes of marlstones , are the hemi- and -pelagic deposits found assigned to facies G2.4. As stated before, internal structures were not clearly visible however, internal structures such as parallelly laminated beds are to be expected. The most distinct features in this facies however was the presence of shell- (bivalvia), pectinidae- and echinoderm-remains.

The distribution curves of grain-size samples taken in the blue marl formation (**Fig. 22**) clearly show a dominance in bell shaped plots of which the most frequent occurring grain-size consists of fine silt (ϕ7, "8 μm"). Furthermore the intermittent frequency distribution, described in facies class D is also clearly present.

Hemipelagic sediments settle vertically through the water column. Its occurrence and formation are resultant from the same controls as for pelagic sedimentation, including; dissolution, productivity and masking *(Reading et al., 1996)*. Hemipelagic advection allows deposition of fine-grained terrigenous material from a variety of sources. Relevant for this stratigraphic unit, as indicated by the grain-size frequency curves, is the addition of the finest portions of low-concentration turbidity currents that can contribute to very dilute suspensions leading to ambient hemipelagic fallout, as described in facies class D.

Pelagic and hemipelagic sediments are generally deposited in low energy, restricted basins. The influence of proximally deposited turbidites aid the supply of terrigenous material, increasing the rate of sedimentation. This facies is most likely deposited in basin plain environments possibly indicating the location of the depo-centre of the basin.

The depositional sequences of the blue marl member are likely to record a regional subsidence that occurred between the two main compressive phases (late Miocene and the Plio-Qaternary respectively) described in the Prerif by *Sani et al., (2007) (Faure Muret and Morel, 1992; Bargach et al., 2004)*.

CLASS B

The facies assigned to Class B consist of deposits with a major sand content that show very few or no alternations with silt to clay sized depositional intervals. The sediments to which this facies is assigned are organized sedimentary sequences consisting of thin- to very thick-beds, in general however medium bed thicknesses are dominant.

Two different facies are recognized in class B: organized fining- (B2.4) and organized coarsening-upward (B2.5) sequences. Their distribution within the class is seemingly sporadic however an increase in coarsening upward beds is recognized upward in stratigraphy.

This facies is made up of composite very fine to medium sized sand beds. Dominant sedimentary structures include: erosional surfaces, parallel-, cross- and through cross-lamination, however few structureless – massive sand beds occur. Only minor bioturbation has been observed. A stratigraphic upward increase in

channel and wedge shaped beds have been recognized that often contained laminated silty rip-up clast at the top and – or at the base of the deposit (**Fig. 10a)**.

Thinsections indicated medium- to highly-spheric, sub-angular to sub-rounded grains in a grain supported fabric. The samples have been classified as litharenites to lithic-wackes. Interestingly, an increase in grain-roundness has been observed in combination with bioclastic material higher up the stratigraphy of section JH-N.

The palaeo-environmental settings of the facies belonging to class B are based not only on the main facies characteristics, however likewise on individual bed characteristics. These facies (B2.4 & B2.5) and hence this stratigraphic unit belong to distal ramp- to basin plain- settings (proximal foreland basin system) with alternating sandy turbiditic deposits influenced and most likely also dominantly reworked by bottom currents.

The *ERICO report (1991)* interpreted this sandy stratigraphic unit as a contourite sequence. The term contourite was originally introduced to specifically define deep sea sediments deposited by contour-parallel thermohaline currents *(e.g. Stow et al., 2002a)*, this definition however has been widened to describe a larger spectrum of sediments affected by various types of bottom currents *(Rebesco et al., 2014)*. Since the definition of contourites is now proposed as a generic term for sediments influenced by bottom currents, the results of this work are in line with the results of the ERICO report. However, bottom currents were not solely responsible for the deposition of this sandy stratigraphic unit.

The transition from facies C2.1, occurring in the JH-N section at 270 m of stratigraphic thickness is marked by an upward increase in mean grain-size from coarse-silt to fine-sand (ϕ5 - ϕ3) as well as an upward increase in the degree of sorting (up to moderately sorted) (**Appendix 4.2**). This sandy stratigraphic unit is furthermore marked by a distinct increase in coarsening upward beds, indicating a possible increased influence of bottom currents upward in stratigraphy.

The increase in palaeo-bathymetry, obtained from biostratigraphic analyses, most likely created palaeo-relief comprising distal ramp- to basin plain- settings at the depositional site. From the fact that this unit is deposited on top of a silty more hemipelagic interval, it is assumed that the overlying deposits (Facies class B) were indeed deposited at or near the depocentre of the basin. The grain-size composition of the sediments however are not typical for low energy basin plain deposits since turbidity currents seldom reach the basin plain *(Reading et al., 1996)*, supporting the hypothesis of the reworking by bottom currents.

Rebesco et al. (2014) indicated that the main types of primary sedimentary structures in contourite deposits consist of thin, delicate structures (up to 10 cm) which is often in sharp contrast to the field observations related to the sand-mud units of this section, which also consisted of structureless sand beds with an average medium thickness. Primary sedimentary structures in contourite deposits however have been observed mainly occurring at the top of the JH – N section consisting of the sandy stratigraphic unit (facies B2) (e.g. Minor erosive surfaces, mud rip-up clasts, upper sharp contacts and bedding features such as cross-bedding). Along with other sedimentary features and the observations related to this sandy stratigraphic unit, a heavily bottom current influenced or entirely reworked turbidite succession is proposed as a palaeo-environmental facies interpretation.

As discussed above, this facies shows an upward change in stratigraphy related to an increase in bottom current influence/velocity on sediment deposition. For this reason, it is suggested that the turbiditic sequence (facies C2.2), which is only slightly influenced by bottom currents and is deposited on the medial- to distal-ramp (occurring at the lower sand-mud unit in this section) changes to a dominantly bottom current influenced basin plain on which these previously sandy medial- to distal-ramp turbidites are transported and re-deposited as sandy contourites.

The wide variety of bottom current influenced deposits indicate that the bottom current velocity altered during the deposition of this statigraphic unit. This alternation in bottom current influence is also observed in the palaeo-current data, that indicated a range of palaeo-current directions mainly oriented W – E but also E – W. A variety of palaeo-current measurements however also indicated slope parallel transport directions which most likely relate to a turbiditic type of deposition. In contrast to the findings of *Ivanovic et al. (2013)* and *Krijgsman et al (1999b)* who showed that Mediterranean water reached the western end of the Rifian Corridor until ~ 6.64

Ma and the corridor was shut between 6.64 – 6.44 Ma, this study indicates that connection and exchange between the Mediterranean and the Atlantic was still occurring.

- *Summary interpretation JH sections* –

Since biostratigraphic results indicated a general increase in bathymetry of the Jebel Haricha section, changes in facies and facies alternations likewise were created by changes in: slope geometry , sediment supply and tectonic intervals. The working hypothesis concerning chronologic alternations of palaeo-environmental changes will shortly be summarized in the following paragraph.

The bottom part of the Jebel Haricha section consists of middle- to distal ramp-settings where high density turbiditic currents were responsible for the deposition of this turbiditic succession. Gradual changes in the source area, possibly created by compressive tectonic quiescence led to a change in the depositional environment. During this period low concentration turbiditic and hemipelagic sediments were deposited. The turbiditic depositional environment got reactivated leading to another sandy turbiditic sequence. A repetition in these facies alternations occurred, however this time the environment remained energetically low for a long period of time, leading to the deposition of the blue marl member. While subsidence remained active and a relative increase in sea-level occurred, changes in the source area led to a similar depositional sequence as determined for the lower part of the section, indicating possibly reactivation of the compressive tectonic forces in the source area. Near the top of the Jebel Haricha composite section, a decrease in energy led, again, to the deposition of mainly hemipelagic and fine grained turbidites. The upper part of the section is marked by a dominantly bottom current controlled environment. Since the source of the sediments does not seem to alter drastically in the entire formation, these bottom current deposits are likely to be reworked or re-deposited turbiditic deposits similar to those described in facies class C.

- *Mahdouma study area (marine)* –

Facies descriptions for the Mahdouma sections are partly similar to the classifications used in the Jebel Haricha composite section concerning the deep-water facies. Sedimentary units deposited above the erosional unconformity have been assigned to alluvial, fluvial and lacustrine depositional environments and are hence treated differently compared to the deep-water facies. *Reading et al. (1996)* has mainly been used to determine the facies and their accompanying palaeo-environmental settings. Since clear facies diagrams as used in the deep water-facies interpretation differ for terrestrial facies, facies names resulted alphabetically from the deep-water facies.

As indicated above, a part of the stratigraphic units found in the Mahdouma study location closely resemble the deep-water deposits of the Jebel Haricha composite section. These stratigraphic units are found in section M – NW and M – SW and mainly consist of marls. In order to fully comprehend the major difference occurring in the deep-water stratigraphic units of the Mahdouma valley, the entire deep-water stratigraphy is shortly described for both sections individually.

Section M – NW consists of 90 meter thick deep-water deposits described to facies G2.4-A, consisting of the blue marl member. A short interval, near the top of section M - NW consists of facies D2.4, as described and interpreted in the discussion concerning the Jebel Haricha section. The grain-size frequency curve and cumulative graph of section M – NW closely resembles the 140 – 205 meter frequency curve and cumulative graph interval of section JH – S, showing an upward increase in the fraction of coarser grains in close proximity to the erosional unconformity.

The results of the grain-size analysis in section M – SW (facies G2.4-B) drastically differ from the results of section M – NW (**Fig. 12, 19, 21, 22 and appendix 4.4**), which is clearly better distributed and consists of a larger percentage of fine grains (**Fig. 12 and 18**). The frequency curves of section M – SW show that the entire deep-water facies of section M – SW closely resemble grain-size results 61 – 140 m of the JH – S section (**Appendix 4.1**), indicating an overall upward decrease in the grain-sizes the composition.

By comparison to the JH sections, the grain-size differences between the deep-water facies of both sections described above seemingly indicate that the deep-water facies of section M-NW are higher in stratigraphy compared to the deep-water facies of section M-SW. This assumption however is in sharp contrast to the field observations that showed dip-directions towards the south, indicating that section M – SW

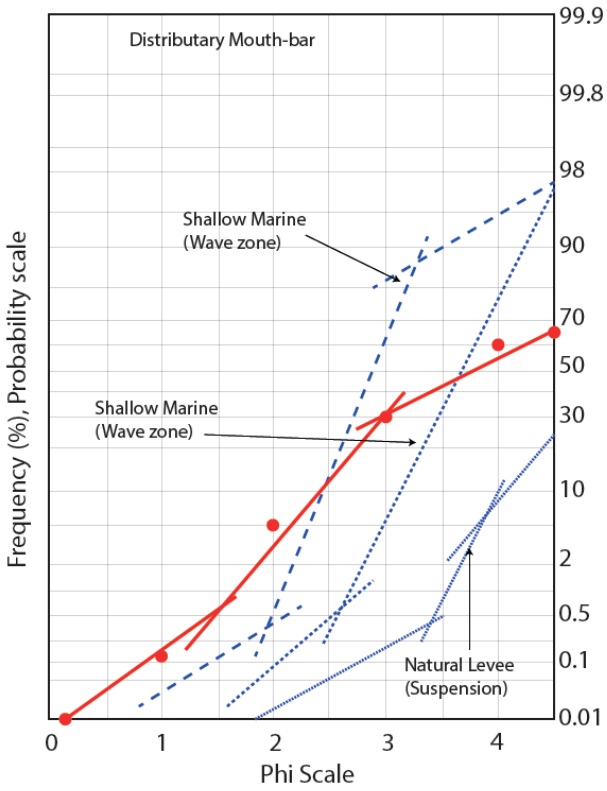

Fig. 23 *Cumulative graph after the findings of Visher (1969) (blue lines). (Red line) findings of this study showing the same trends, however with a different range of grain-sizes.*

is stratigraphically located above section M - NW. Furthermore, it can be concluded that comparison between the JH and M sections is nearly impossible with present knowledge.

Section M –SE, located roughly at the middle of the eastern flank consists of a thickening up-ward silty sand sequence. This silty-sand sequence contained: minor bioturbation, cross- and through cross-bedding as well as several shell remains (Spec. Ostreidae). Since this depositional unit has not been carefully logged, an approximation of the stratigraphic thickness is made based on the lateral difference between 4 study locations. For this reason, it is noted that the stratigraphic heights concerning this section is mere meant as an indication of the height difference between studied outcrops.

Approximately 10 meter up in stratigraphy, throughs/channels and reworked grey – red silty layers were recognized. The average wavelength of bedforms was 2.5 – 3 m and bed thicknesses ranged from 5 to 40 cm. Furthermore, these sedimentary deposits contained sandy rip-up clasts (max. 2 cm) and were moderately bioturbated.

At an estimated stratigraphic height of 40 meters, an increase in shell-fragment size and amount was observed. Furthermore the average bed-thickness of 60 cm increased to an average thickness of 2 m, which hover might be composed of multiple, similarly looking layers. The orangish silty-sands observed in this section contained laminated gray and more reddish silt intervals.

Despite minor (max. 0.2 ϕ) differences in mean-grainsize between bottom and top samples, the beds are fining up-ward. The internal bed structures of section M – SE can be described as; well distributed very poorly sorted.

Section M – SE could not visibly be connected to the surrounding sections found in the Mahdouma valley. The occurrence of *Ostreidae* shell remains, although only present in small amounts, hint to a marine environment, most likely placing this stratigraphic unit below the unconformably deposited conglomeratic limestone sequences. The deep-water facies found at the western side of the valley do not include a clearly visible transition to the stratigraphic unit belonging to the M – SE section. Grain-size results however give an indication of a possible gradual transition from the clayey silt found in section M – NW to the silty sand of section M – SE.

As discussed before, the cumulative curve belonging to the deep-water facies (G2.4 A) in section M – NW (**Fig. 12**) shows a gradual increase in the percentage of sand continuing in the deep-water facies (G2.4 B) belonging to section M – SW, indicating a possible transition from the clayey-silt to the sandy-silt and silty-sand found in section M – SW. Section M – SW, in turn could be related to section M – SE by a gradual transition from sandy-silt and silty-sands found in section M – SW to silty-sands deposited in section M – SE (**Fig. 12**). Despite remaining uncertainties of the possibility that the silty-sand unit of section M – SE is stratigraphically related to the deep-water facies found at the western side of the valley, no better alternative of the stratigraphic location of section M – SE has been found.

When comparing the cumulative frequency grain-size curves of the M – SE section to the curves produced by *Visher (1969)* (**Fig. 23**) it shows that the trends relate to shallow marine environments, furthermore, since the results of *Visher* were obtained in shallow marine settings close to a distributary system the results may indicate high rates of sediment supply. These relative shallow marine environments were also recognized by the presence of *Ostreidae*. The curves of *Visher* however show drastically lower

amounts of fine grained particles. Examples of grain-size distributions in near coastal- sand deposits show moderately to very well sorted sediments mainly due to winnowing processes by wave agitation *(e.g. Friedman, 1979; Visher, 1969).* Since the majority of the grain-size samples show positively skewed size-frequency distributions (**Appendix 4.5**), the samples indicate a lack in strong winnowing action that normally occurs in open, shallow marine settings *(Friedman, 1979)*. The lack in winnowing and restricted marine features indicate that the sediment have clearly been deposited below zones prone to winnowing. The presence or influence of waves in this restricted environment was possibly very low. During the field trip the discussion arose of the possible occurrence of hummocks, which is an indication that during periods of intense, storm related weather, the wave base reached the deposited sediments, favoring the theory of a relatively shallow marine environment.

Since the palaeo-currents, mainly related to small scale crossbedding, indicated dominant ENE and ESE transport directions (**fig**. **24**) it is assumed that these currents are related to possible bottom currents, which in turn are related to the exchange of Atlantic and Mediterranean sea-water, as is the case for the upper JH-N deposits.

- *Mahdouma study area (non-marine)* –

Although the probably Late Pliocene deposits are relatively unimportant for this study, they have been logged and studied in detail. For this reason, they might be interesting for other studies and hence they are shortly discussed.

Essahlaoui (2001) and *Sani et al. (2007)* found blue marls unconformably overlain by shallow marine or littoral sands. These shallow marine or littoral sands are in turn overlain by lacustrine limestones in the Saïss Basin. In contrast to their findings, at the western flank of the Mahdouma valley lacustrine limestones are unconformaly deposited on top of relatively deep, below wave base- marine facies. The lacustrine limestones of the Saïss Basin were first described by *Taltasse (1953)*, who also precisely evaluated the extension of the lake in which these limestone successions were deposited. *Taltasse (1953)* furthermore indicated that the lacustrine limestones were deposited in the Saïss Basin during Late Pliocene times.

The first facies deposited unconformably on top of the deep-water facies in section M – SW consists of a conglomerate with a bioclastic, carbonate coated matrix that has a high content of tube shaped, up to 0.5 cm clast which are believed to be calcified charophytic stems. The well rounded clast sizes range from 2 – 7 cm and are generally deposited fining up-ward. Individual beds have medium to thick bed-thicknesses and the main sedimentary structures are channel shapes (erosive bottoms) and cross-bedding. This facies is marked by a gradual fining up-ward sequence.

Based on a scheme for conglomeratic alluvial facies by *Reading et al. (1996) (after Ramos & Sopeña)*, the sedimentary structures recognized in facies H.1 indicate stratified complex channel fill. Since this facies is deposited unconformably on top of the deep-water facies it can be concluded that the previous environment was dominantly erosional. Furthermore, the base of this conglomeratic limestone shows erosional features as well, indicating that erosion was aided by the depositional environment of this facies. The matrix, which mainly consisted of bioclastic and possibly of carbonate coated clastic grains is believed to have formed in lacustrine environments. Since this depositional sequence has not been deposited on top of lacustrine deposits, both the clasts and the matrix were transported from a lacustrine-, or previously lacustrine-environment. Another possible scenario however, can be that the mainly mud-rich clasts were transported through, and eroded a previously shallow marine, littoral or lagoonal environment which were encountered in previous studies in the Saïss Basin *(e.g. Essahlaoui, 2001 and Sani et al., 2007)* of which the latter is also known to produce Charophyta. This study lacks sufficient data to conclude the nature and the origin of the matrix, however the deposits in this facies are determined to be channel-fill conglomerates created by fluvial fans.

Both northern sections in the Mahdouma valley, sections M – NW and M – NE show the presence of facies H.2. Facies H.2 are characterized by mainly thick (~ 1m), fining up-ward clastic sequences with high carbonate content. This stratigraphic unit has channel, and slightly wedge shaped beds with cross- and parallel- lamination and laminated intervals with coarser, often bioclastic material (charophytc tubes). The coarser occurring clasts (up to granule) consist of mudstones and oncoids, whereas the finer grained intervals are moderately

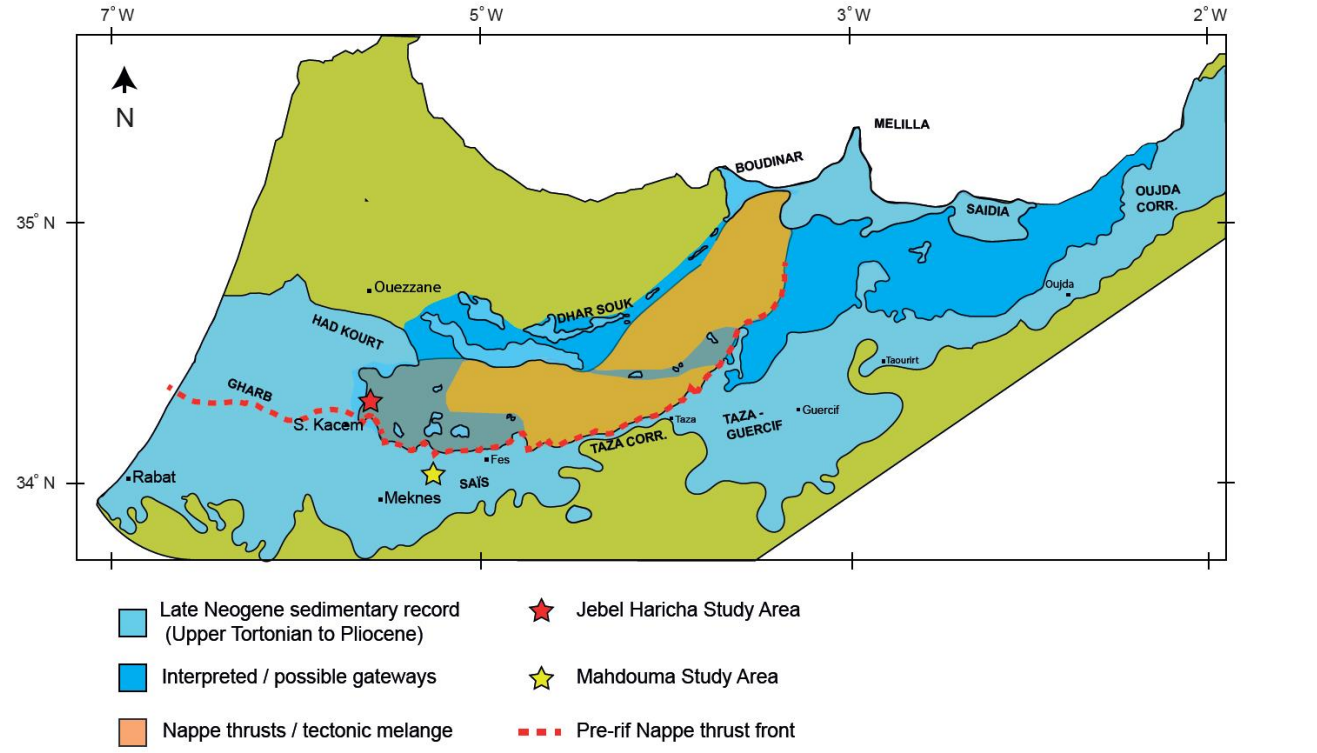

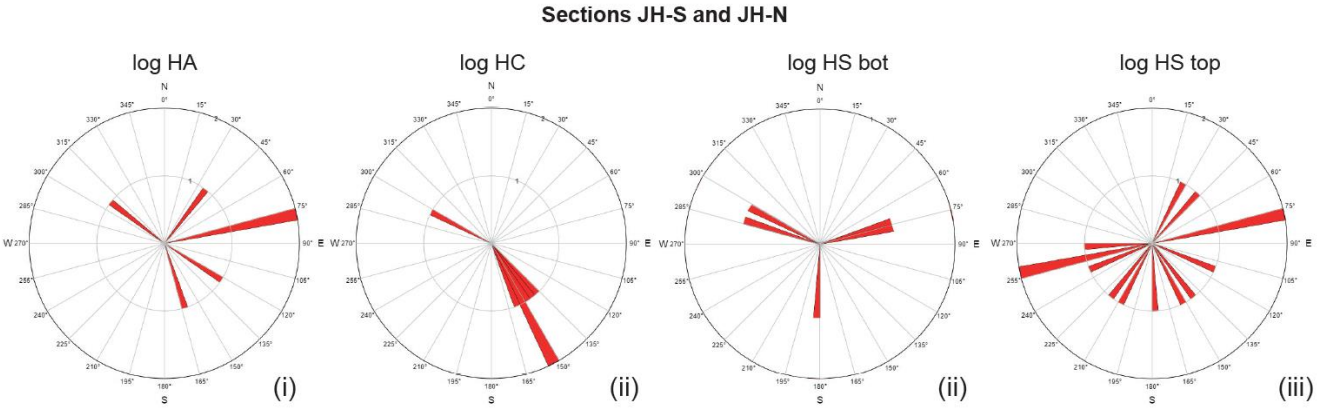

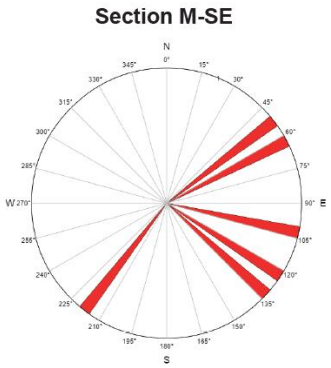

Fig. 24 (top) *Interpretation of the Rifian Corridor geometry, modified after W. Capella (2015). Note that the Nappe thrust was submerged allowing the deposition of deep-marine deposits on top of the tectonic melange, as found in the stratigraphy of the Jebel Haricha section.*

(bottom) *Palaeo-current directions. The transport directions obtained from the Jebel Haricha sections (sections JH-S and JH-N) have been corrected for rotation. The palaeo-current directions for the Mahdouma section (section M-SE) were argued not to be influenced by post depositional rotation.*
Red lines indicate palaeocurrent directions (towards outer circle). For the Jebel Haricha sections, longer lines indicate that the same direction is measured twice.

bioturbated. Furthermore, a laterally occurring palaeosoil was found in this facies in section M – NE.

The often light beige to orange coloured stratigraphic unit belonging to facies H2.2 is described to a fluvial to lacustrine environment. The Sheetflood fan deposits and horizontally stratified sedimentary features are occurent in alluvial fans (Nichols, 2009). A stratigraphic change from stream channel fans and braided stream facies to energetically lower environments where mottled marly intervals are deposited, described to more lacustrine and floodplain environments, (Tucker, 2001) occurred. This stratigraphic unit, as well as the stratigraphic unit of facies H.1 was deposited in a fresh water system since signs of

evaporate deposits are lacking.

Facies J.1 (**Fig. 12**) is characterized by an alternation of indurated granular conglomeratic packstones, with paralelly laminated fining-upward beds and red coloured organic material and rootlet containing paleosoils. The matrix of the conglomeratic beds consist of carbonate coated clastic material that is slightly orange colored. This facies interval occurs in section M – SW, between two stratigraphic units belonging to facies H.1 and is 5 meters thick.

The palaeo-environmental of facies J.1 is characterized by an alternation of "dry" and "wet" conditions. The granular conglomeratic grainstone has an alluvial origin, comparable with facies H.1 although with a reduced clast size. The grainstone characteristics of this conglomeratic limestone can possibly explained by a depositional setting in a lacustrine environment ("wet" conditions). After the deposition of these granular sized deposits in low-energy, wave- or current-agitated zones (Reading et al., 1996), these deposits could have been disposed of the very finest matrix resulting in what remains as a conglomeratic grainstone. The alteration with paleosoils indicates changes in relative water-level, showing that "dry" periods must have occurred, favouring the formation of paleosoils.

Facies J.2, which might be the lateral equivalent of facies J.1 consists of slightly channel or wedge shaped, sub-horizontally bioturbated, oncoid rich, fine-grained sandstones in alternation with oncoide rich grainstones. As oncoids form in shallow, gently wave-agitated zones under the occurrence of green algae and cyanobacteria (Nichols, 2009) and lacustrine grainstones form in low energy water bodies as well (Reading et al., 1996), the stratigraphic changes are related to changes in sediment supply. As previously stated, this facies might resamble a lateral variation of facies J.1 which was argued to consist of an alluvial, possibly deltaic system deposited in a shallow lacustrine environment. Facies J.2 can be explained as the finer grained lateral equivalent of this alluvial system.

6.2 Palaeo-current results and interpretation

Palaeo-current directions determined in the Jebel Haricha composite section are categorized in three stratigraphic units: (i) the pre-blue marl member turbiditic succession mainly composed of facies group C2, (ii) the post blue marl member turbiditic succession mainly composed of facies group C2 and (iii) the upper, bottom current influenced stratigraphic unit belonging to facies group B2 (**Appendix 2.1**).

The palaeo-current data of the lowermost C2 facies group indicate dominantly eastward oriented transport directions with a dispersed N – S component. Since contourite current indications are lacking, it is assumed that the diversity of palaeo-current directions is created by the route- and outward radiating directional characteristics of palaeo-current deposits. If however this stratigraphic unit was affected by slope perpendicular currents, it is characterized by an Atlantic to Mediterranean flow regime.

In comparison to (i), the post- blue marl member turbiditic sequence (ii, C2.2) also lacked bottom current indicators. This palaeo-current interval is marked by a dispersed flow regime as well, the major current indicators however showed a dominantly southward oriented transport direction. Furthermore slope parallel currents have been observed indicating bi-directional, both E-W and W-E transport directions. As explained in the section describing (i), this slope perpendicular transport direction is possibly created by the geometry of sediment deposition from turbiditic currents, which often radiate outward parallel to the slope.

Despite the lack in bottom current indicators in both (i) and (ii) the function of the Rifian Corridor consists of water exchange between the Atlantic Ocean and the Mediterranean. For this reason it might be likely that bottom currents did occur. *Ivanovic et al. (2013)* and *Krijgsman et al (1999b)* however, showed that Mediterranean water reached the western end of the Rifian Corridor until ~ 6.64 Ma and the corridor was shut between 6.64 – 6.44 Ma.

Based on the timing of closure and the end of water exchange between the Mediterranean and the Atlantic Ocean, it can be concluded that during the time of deposition of this composite section bottom currents created by water exchange and saline density currents could not have existed. If their finding were right, the section should have been deposited in a very restricted environment where bottom current activity would have been significantly less compared to an active corridor. The upper-most stratigraphic unit of the Jebel Haricha composite section (iii) however, has clearly been affected by bottom currents, favoring the presence of an active gateway.

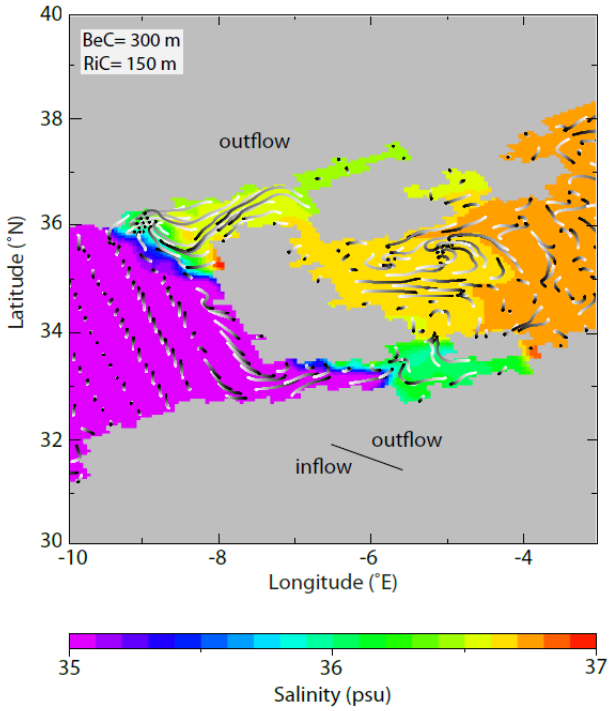

Fig. 25 *Figure of the modelled water fluxes between the Atlantic and the Mediterranean. The figure uses salinity as a tracer to distinguish between the inflow and outflow in the gateway area. Low salinity corresponds to the Atlantic inflow and higher salinity to the Mediterranean outflow. The figure shows salinity (psu) and flow trajectories at the seafloor in the gateway area. Trajectories show the paths water would travel in 30 days. Tails are white and heads are black. The Betic Corridor is set to 300 m - and the Rifian Corridor to 150 m depth. From: De La Vera (2015).*

The contourite rich stratigraphic unit (iii) shows both E – W and W – E palaeo-current directions indicating the possibility of both Atlantic – Mediterranean and Mediterranean – Atlantic flow regimes. Furthermore highly dispersed palaeo-current measurements indicate a mainly southward trend, which is indicative for possible down slope movement. When these palaeo-current measurements are related to currents related to water exchange between the Atlantic and the Mediterranean, they indicate that these water masses were connected up to 6.29 Ma, although connection could have been much more restricted than before.

Martín et al. (2001) state that the Guadalhorce gateway, the only Messinian Betic strait, is believed to have been coeval with the Rifian Corridor. They found that the circulation patterns within the Guadalhorce gateway are characterized by bottom currents flowing from the Mediterranean into the Atlantic. According to *Benson et al. (1991)*, who proposed the 'siphon' model, Atlantic waters entered the Mediterranean through the Rifian Corridor, while saline currents from the Mediterranean flowed out through a Betic discharge channel. Atlantic – Mediterranean communication however became restricted to the Rifian Corridor after closure of the Guadalhorce gateway during Early Messinian *(Martín et al., 1999)*.

Ivanovic et al. (2012) stated that data from the Taza-Guercif and Melilla basins, located in northern Morocco, age constraints were determined to the age of Rifian Corridor closure (6.64-6.44 Ma). Furthermore they state that no evidence was found for the 'siphon' model introduced by *Benson et al. (1991)*. In contrast to their first statement, they indicate that their results cannot exclude the possibility that at times during the Messinian Salinity Crisis, Mediterranean outflow waters reached the Atlantic. This statement is only one of several example of uncertainties related to the exact timing of closure in the Rifian Corridor, aiding the possibility that water exchange between the Atlantic and the Mediterranean could have created the bottom currents that affected sedimentation in the Jebel Haricha section.

The possibility of a remaining connection between Atlantic and Mediterranean waters is backed by *Rouchy and Caruso (2006)* who reassessed the data concerning the MSC in the Mediterranean basin. *Rouchy and Caruso (2006)* stated that reduced inputs of seawater continued to enter at least episodically the Mediterranean basin through the MSC explaining the sporadic presence of marine organisms. These Atlantic water inputs reached their lowest value and practically ceased during the latest Messinian, just before the abrupt restoration of stable open marine conditions at the beginning of the Zanclean.

It is argued that the Rifian Corridor was still open at the time of deposition (6.39 – 6.29 Ma) of the Jebel Haricha sections. The Mahdouma sections however have not been dated. Since the blue marl member was recognized in both sections it is assumed that the timing of deposition of the Mahdouma – marine units was in close proximity to the time interval determined for the Jebel Haricha sections.

Assuming that the relatively shallow marine, deposits found in section M-SE are dated to be deposited 6.39 – 6.29 Ma it can be concluded that bottom currents found in both study locations belong to the same process of Mediterranean –

Atlantic water exchange. *(An indication of palaeo-current velocities can be found in **Appendix 7**)*

The model study of *de la Vara et al. (2015)* concerning the Atlantic – Mediterranean water fluxes prior to the MSC shows that, when two gateways exist (i.e., Betic and Rifian corridors), both corridors show inflow and outflow except when the shallower of the two corridors is shallower than the mid-depth of the deep corridor. In this case the shallow corridor accommodates only inflow from the Atlantic. This model study also shows that in wide sections of the gateway Coriolis force acts and causes water accumulation to the right of the flow trajectory. As a result of rotation of flows due to Coriolis force, at some locations in the gateway, the inflow-outflow interface reaches the bottom and in- and outflow occur side by side at the seafloor (**Fig. 25**).

Combining the findings of *de la Vara et al. (2015)* with the palaeo-current directions obtained in this study, inflow may have occurred to the south (Mahdouma) and outflow to the north (Jebel Haricha). This however involves the important assumption that the observations are at all representative of the time-averaged flows obtained from the model. The fact that both in- and outflow have been documented in the JH-N section could be caused by the location of these deposits, which are in the central part of the gateway close to the expected location of the inflow-outflow interface. Small changes in the configuration of the gateway area, the climatic conditions or natural variability of the flow system could slightly alter the position of the interface which in turn could be the cause of the bi-directional palaeo-current directions recorded in the deposits.

However, in the model study by *de la Vara et al. (2015)*, the interface is never able to reach the seafloor when there is only one Mediterranean-Atlantic connection. More specifically, side-by-side flow at the bottom only occurs in the shallower of the two corridors, where the interface is closer to the bottom due to relatively shallow settings. The authors point out two possibilities (*Alba de la Vara, personal communication*): (1) another corridor was open and the corridor comprising the study areas was the shallower of the two connections or (2) the Rifian Corridor was wider than the width they use in their calculations (the wider the gateway the more important rotational effects become).

As a final remark to the discussion on the duration of Rifian Corridor water exchange I would like to indicate one of the main questions related to the MSC: how could this thick evaporitic sequence be deposited in such a short period of time?. A constant supply of salt (Atlantic water) could have significantly aided the increasing salinity and the amount of salt present in the Mediterranean, favoring the rate and amount of salt accumulation at the bottom of the Mediterranean basin.

7. LIMITATIONS AND WEAKNESSES

Due to a lack in field-time a lot of assumptions were made in the discussion. The lack of field-time affected mainly the amount of samples and palaeo-current indicators gathered as well as the documentation concerning section M-SE. Furthermore, the study would have profoundly benefitted from the addition of one or more study areas.

Since the biostratigraphic samples could not have yet be analyzed, assumptions were made concerning the timing of deposition of the Mahdouma sections. When the assumptions concerning the timing of deposition of the marine facies in the Mahdouma section prove wrong, this could greatly influence the interpretation of the discussed contributors to palaeo-current indicators found in the Mahdouma section, as well as its interpretation related to the findings of *de la Vara et al. (2015)*.

8. FUTURE WORK

Since the geometry of the Rifian Corridor is not yet fully understood, mainly concerning the width and depth changes of the Rifian Corridor prior, and during the Mediterranean Salinity Crisis, it is recommended to enhance the amount of study areas near the locations described in this study. The increase in amount of study areas will strongly benefit the study of *de la Vera et al. (2015)* as well, since it can provide answer to one of the two possible scenario's proposed.

Besides increasing the amount of study locations, it will also be beneficial to improve the knowledge on the source of the monotonous sediment supply found in this study. The monotonous sediment supply within the sections proved rather difficult to explain. For this reason I would like to suggest a detailed study concerning

mainly the source and the way of transport towards the basin (e.g. windblown or water-transported). This study would improve the knowledge and understanding of sedimentation in the basin, as well as the processes responsible for the seemingly phase related sediment supply. Furthermore, the results can provide profound knowledge concerning the closure of the Rifian Corridors and the influence of currents throughout the gateway.

9. IMPORTANCE OF THIS WORK

Besides the limitations and weaknesses of this study, it provides a proper framework for present and future studies concerning the Mediterranean Salinity Crisis. This study indicated that sea-water exchange, and hence gateway related processes still occurred between, at least 6.39 and 6.26 Ma, providing important knowledge to the processes leading to the MSC and closure of the Rifian Corridor. Furthermore, the findings, interpretations and hypothesis described in this thesis will benefit the understanding of gateway related processes. But, above all, this study enhances the availability of sedimentary logs, biostratigraphic-, magnetostratigraphic-, and grain-size results and interpretations that can be used for reassessment of previous, as well comparison material for future studies related to the Rifian Corridor and the MSC. Finally, in a more general way, this work is a case study concerning sedimentary infilling patterns of a foreland basin.

10. CONCLUSION

The stratigraphic successions studied in both the Jebel Haricha as the Mahdouma sections show deep-marine deposits related to the Rifian Corridor, deposited at a time interval that range from 6.37 to 6.29 Ma. The stratigraphic successions between both locations can be distinguished by two turbiditic succession in the Jebel Haricha section and an unconformably deposited alluvial to lacustrine succession deposited on top of deep-marine facies in the Mahdouma sections.

The onset of turbidite deposition is engendered by the subsidence phase which post-dates the Nappe emplacement. The lithological make-up shows alternations related to tectonically induced changes. These changes, which most likely occurred in the region of the source rocks indicate differences in tectonic activity that occurred in two phases. The first phase is marked by a decrease in tectonic activity, eventually leading to the deposition of the blue marl member. The second phase was recorded as an increase in tectonic activity following the deposition of the blue marl member.

The data collected from both study areas indicate that the Mediterranean and the Atlantic were still connected at 6.37 to 6.29 Ma, enabling water-exchange between the two.

Biostratigraphic results indicated a deepening trend of the basin, which ruled out the possible occurrence of shallow marine deposits. The upper-most marine stratigraphic unit of both composite sections (Jebel Haricha and Mahdouma) show signs of bottom current deposits or bottom current influenced deposits. The palaeo-current directions, deducted from transport directions indicate a bi-directional (E-W and W-E) flow regime in the Jebel Haricha section and a dominant eastward bottom current direction in the Mahdouma section.

The difference between palaeo-current directions of the Jebel Haricha and the Mahdouma sections analyzed by the results of a model concerning water fluxes related to the Rifian Corridor led to two options concerning the geometry of the corridors connecting the Atlantic and the Mediterranean around 6.29 Ma. These two hypothetical scenarios include: (1) another corridor was open and the corridor comprising the study areas was the shallower of the two connections or (2) the Rifian Corridor was wider than the width used in the model calculations. This analyses indicates that the geometry of the Rifian Corridor differs from what is generally assumed (**Fig. 1.a**).

ACKNOWLEDGEMENTS This work strongly benefitted from the syn-fieldwork supervision and discussions with W. Capella, Dr. L.C. Matenco and Dr. J. Trabucho Alexandre, who are furthermore also warmly thanked for their post-fieldwork supervision, guidance, help with several aspects of this study and improving this manuscript. Prof. Dr. W. Krijgsman is warmly acknowledged for supervising this master thesis, helping to improve this manuscript and guidance during magnetostratigraphic analysis. J. Eggenhuisen is acknowledged for his contribution concerning the discussion on interpretation and influence of the marine gateway. M.A. Tulbure is acknowledged for her contribution concerning the biostratigraphic analyses and results. T. Zalm is thanked for his joyful help and supervision during the grain-size analysis experiment in the Geo Laboratory. A. De La Vera is acknowledged for the personal communication and explanation concerning her findings related to Mediterranean and Atlantic water exchange. Mr. A.M. Kouissi is acknowledged for his help during the Moroccan fieldwork, both in the field the kitchen and administrative. At last I want to especially thank my partner and colleague M. van Oorschot for conducting the fieldwork, bringing a CD of Paul Simon along and for conducting several of the experiments with me. This research has been founded by EU Marie Curie, for which they are gratefully acknowledged.

REFERENCES

Ahmamou, M., & Chalouan, A. (1988). Distension synsédimentaire plio-quaternaire et rotation anti-horaire des contraintes au Quaternaire ancien sur la bordure nord du bassin du Saïss (Maroc). *Bull. Inst. Sci. Rabat*, *12*, 19-26.

Ait Brahim, L., & Chotin, P. (1989). Genèse et déformation des bassins néogènes du Rif central (Maroc) au cours du rapprochement Europe-Afrique.*Geodinamica Acta*, *3*(4), 295-304.

Bargach, K., Ruano, P., Chabli, A., Galindo-Zaldívar, J., Chalouan, A., Jabaloy, A., ... & Benmakhlouf, M. (2004). Recent tectonic deformations and stresses in the frontal part of the Rif Cordillera and the Saïss Basin (Fes and Rabat regions, Morocco). *pure and applied geophysics*, *161*(3), 521-540.

Benson, R. H., Bied, R. E., & Bonaduce, G. (1991). An important current reversal (influx) in the Rifian Corridor (Morocco) at the Tortonian-Messinian boundary: The end of Tethys Ocean. Paleoceanography, 6(1), 165-192.

Boggs, S. (2009). Petrology of sedimentary rocks. Cambridge University Press.

Bonnecaze, R. T., Huppert, H. E., & Lister, J. R. (1993). Particle-driven gravity currents. Journal of Fluid Mechanics, 250, 339-369.

Boutakiout, M. (1990) Les foraminifères du Jurassique des Rides Sud-Rifaines et des regions voisines (Maroc). Doc des Lab Géol Lyon 112:1-247.

Bruderer, W., Gouskov, N., Gubler, J., Jacquemont, P., Levy, R., & Tilloy, R. (1950). Carte géologique régulière du Maroc au 1: 100.000: Fès Ouest. *Soc. Cherif. Petroles, Notes et Mémoires Services Géologique Maroc*, (109).

Carte Ge´ologique du Maroc (1985) Royaume du Maroc, Ministe`re de l'Energie et des Mines, Direction de la Ge´ologie. Publ. 260 du Service Ge´ologique du Maroc (scale 1:1,000,000)

Chenakeb, M. (2004). Carte Géologique du Maroc, Feuille Beni Ammar, echelle 1: 50.000. *Notes Mem Serv Géol Maroc*, *428*.

Daguin, F. (1927). *Contribution à l'étude géologique de la région prérfiaine (Maroc occidental)*. impr. l'Abeille, 14, avenue de Toulouse.

Essahlaoui, A., Sahbi, H., Bahi, L., & El-Yamine, N. (2001). Preliminary survey of the structure and hydrogeology of the western Saiss Basin, Morocco, using electrical resistivity. Journal of African Earth Sciences, 32(4), 777-789.

Faugères, J. C. (1978). *Les Rides sud-rifaines: Evolution sédimentaire et structurale d'un bassin atlantico-mesogéen de la marge africaine* (Doctoral dissertation).

Faugères, J. C. (1981). Evolution structurale d'un bassin atlantico-mesogeen de la marge africaine; les rides Sud-rifaines (Maroc). *Bulletin de la Société Géologique de France*, (3), 229-244.

Faure Muret A, Morel JL (1992) Carte Néotectonique due Maroc 1:100.000. Feuille 1: Provinces du Nord. Notes Mem Serv Géol Maroc 368.

Feinberg, H. (1986). *Les Séries tertiaires des zones externes du Rif (Maroc): biostratigraphie, paléogéographie et aperçu tectonique* (No. 315). Éditions du Service géologique du Maroc.

Flinch, J. F. (1996). Accretion and extensional collapse of the external Western Rif (Northern Morocco). *Mémoires du Muséum national d'histoire naturelle*, *170*, 61-85.

Folk, R. L., & Ward, W. C. (1957). Brazos River bar: a study in the significance of grain size parameters. Journal of Sedimentary Research, 27(1).

Folk, R. L., Andrews, P. B., & Lewis, D. (1970). Detrital sedimentary rock classification and nomenclature for use in New Zealand. New Zealand journal of geology and geophysics, 13(4), 937-968.

Friedman, G. M. (1979). Differences in size distributions of populations of particles among sands of various origins: addendum to IAS Presidential Address. Sedimentology, 26(6), 859-862.

Frizon de Lamotte, D., Crespo-Blanc, A., Saint-Bézar, B., Comas, M., Fernàndez, M., Zeyen, H., ... & Michard, A. (2004). TRASNSMED-transect I [Betics, Alboran Sea, Rif, Moroccan Meseta, High Atlas, Jbel Saghro, Tindouf basin]. *Cavazza W., Roure F., Spakman W., Stampfli GM & Ziegler PA (éds.)–The TRANSMED Atlas-the Mediterranean region from Crust to Mantle*.

Hsü, K. J. (1972). When the Mediterranean dried up. *Scientific American*, *227*, 26-36.

Hsü, K. J., Ryan, W. B. F., & Cita, M. B. (1973). Late Miocene desiccation of the Mediterranean. *Nature*, *242*(5395), 240-244.

Hsü, K. J., Montadert, L., Bernoulli, D., Cita, M. B., Erickson, A., Garrison, R. E., ... & Wright, R. (1977). History of the Mediterranean salinity crisis. *Nature*,*267*(5610), 399-403.

Ivanovic, R. F., Flecker, R., Gutjahr, M., & Valdes, P. J. (2013). First Nd isotope record of Mediterranean–Atlantic water exchange through the Moroccan Rifian Corridor during the Messinian Salinity Crisis. Earth and Planetary Science Letters, 368, 163-174.

Johansson, M., Braakenburg, N. E., Stow, D. A., & Faugères, J. C. (1998). Deep-water massive sands: facies, processes and channel geometry in the Numidian Flysch, Sicily. Sedimentary geology, 115(1), 233-265.

Kelts, K. (1981). Turbidites After Ten Years of Deep Sea Drilling Wringing Out the Mop.

Krijgsman, W., Hilgen, F. J., Raffi, I., Sierro, F. J., & Wilson, D. S. (1999). Chronology, causes and progression of the Messinian salinity crisis. *Nature*,*400*(6745), 652-655.

Krijgsman, W., Gaboardi, S., Hilgen, F. J., Iaccarino, S., Kaenel, E. D., & Laan, E. V. D. (2004). Revised astrochronology for the Ain el Beida section (Atlantic Morocco): no glacio-eustatic control for the onset of the Messinian Salinity Crisis. Stratigraphy, 1, 87-101.

Kranck, K. (1984). Role of flocculation in the filtering of particulate matter in estuaries. The Estuary as a Filter, Academic Press, Orlando FL. 1984. p 159-175, 6 fig, 44 ref.

Krumbein, W. C. (1937). Sediments and exponential curves. The Journal of Geology, 577-601.

Langereis, C. G., Krijgsman, W., Muttoni, G., & Menning, M. (2010). Magnetostratigraphy–concepts, definitions, and applications. *Newsletters on Stratigraphy*, *43*(3), 207-233.

Laville, E. D. G. A. R. D., & Pique, A. L. A. I. N. (1991). La Distension crustale atlantique et atlasique au Maroc au debut du Mesozoique; le rejeu des structures hercyniennes. *Bulletin de la Société géologique de France*, *162*(6), 1161-1171.

Laville, E., Pique, A., Amrhar, M., & Charroud, M. (2004). A restatement of the Mesozoic Atlasic rifting (Morocco). *Journal of African Earth Sciences*, *38*(2), 145-153.

Litto, W., Jaaidi, E., Medina, F., & Dakki, M. (2001). Seismic study of the structure of the northern margin of the Gharb Basin (Morocco): Evidence for a late Miocene distension. *Eclogae Geologicae Helvetiae*, *94*(1), 63-74.

Martín, J. M., Braga, J. C., & Betzler, C. (2001). The Messinian Guadalhorce corridor: the last northern, Atlantic–Mediterranean gateway. Terra Nova, 13(6), 418-424.

Martín, J. M., Braga, J. C., & Sánchez-Almazo, I. (1999). The Messinian record of the outcropping marginal Alboran basin deposits: significance and implications.

Michard, A. (1976). Eléments de géologie marocaine (Vol. 252). Éditions du Service géologique du Maroc.

Michard, A., Saddiqi, O., Chalouan, A., & de Lamotte, D. F. (Eds.). (2008). Continental evolution: The geology of Morocco: Structure, stratigraphy, and tectonics of the Africa-Atlantic-Mediterranean triple junction (Vol. 116). Springer Science & Business Media.

Morel, J.L. (1989) Etats de contrainte et cinématique de la chaine rifaine (Maroc) du Tortonien à l'actuel. Geodinamica Acta 3:238-294.

Mutti, E., & Ricci Lucchi, F. (1972). Le torbiditi dell'Appennino settentrionale: introduzione all'analisi di facies. Memorie della Societa Geologica Italiana, 11(2), 161-199.

Nichols, G. (2009). Sedimentology and stratigraphy. John Wiley & Sons.

Olsen, P. E. (1997). Stratigraphic record of the early Mesozoic breakup of Pangea in the Laurasia-Gondwana rift system. *Annual Review of Earth and Planetary Sciences*, *25*(1), 337-401.

Pettijohn, F. J. (1987). Sand and sandstone. Springer Science & Business Media.

Pickering, K., Stow, D., Watson, M., & Hiscott, R. (1986). Deep-water facies, processes and models: a review and classification scheme for modern and ancient sediments. Earth-Science Reviews, 23(2), 75-174.

Reading, H. G. 1996, Sedimentary Environments; Processes, Facies and Stratigraphy.

Reading, H. G., & Richards, M. (1994). Turbidite systems in deep-water basin margins classified by grain size and feeder system. AAPG bulletin, 78(5), 792-822.

Rebesco, M., Hernández-Molina, F. J., Van Rooij, D., & Wåhlin, A. (2014). Contourites and associated sediments controlled by deep-water circulation processes: State-of-the-art and future considerations. Marine Geology, 352, 111-154.

Rouchy, J. M., & Caruso, A. (2006). The Messinian salinity crisis in the Mediterranean basin: a reassessment of the data and an integrated scenario.*Sedimentary Geology*, *188*, 35-67.

Sani, F., Del Ventisette, C., Montanari, D., Bendkik, A., & Chenakeb, M. (2007). Structural evolution of the Rides Prerifaines (Morocco): structural and seismic interpretation and analogue modelling experiments. *International Journal of Earth Sciences*, *96*(4), 685-706.

Shepard, F. P. (1954). Nomenclature based on sand-silt-clay ratios. Journal of Sedimentary Research, 24(3).

Sierro, F. J., Flores, J. A., Civis, J., Gonza, J. A., & France, G. (1993). Late Miocene globorotaliid event-stratigraphy and biogeography in the NE-Atlantic and Mediterranean. Marine Micropaleontology, 21(1), 143-167.

Stow, D. A., Faugères, J. C., Viana, A., & Gonthier, E. (1998). Fossil contourites: a critical review. Sedimentary Geology, 115(1), 3-31.

Stow, D. A., Faugères, J. C., Howe, J. A., Pudsey, C. J., & Viana, A. R. (2002). Bottom currents, contourites and deep-sea sediment drifts: current state-of-the-art. Geological Society, London, Memoirs, 22(1), 7-20.

Taltasse, P. (1953) Recherches géologiques et hydrogéologiues dans le Bassin lacutre de Fes-Meknès. Notes Mem Serv Géol Maroc 115:1-300.

Tilloy R (1955) Notice de explicative de Feuille Fes-ouest de la Carte Geologique du maroc au 1:100.000. Notes Mem Serv Géol Maroc 109:1-62

Tucker, M. E. (2001). Sedimentary Petrology.-272 pp.

Visher, G. S. (1969). Grain size distributions and depositional processes. Journal of Sedimentary Research, 39(3).

Zijderveld, J. D. A. (1967). AC demagnetization of rocks: analysis of results. Methods in paleomagnetism, 3, 254.

Zizi, M. (1996). Triassic-Jurassic extensional systems and their Neogene reactivation in Northern Morocco (the Rides Prerifaines and Guercif basin).*Notes et mémoires du service géologique du Maroc*, (416).

Zizi, M. (1996b). Triassic-Jurassic extension and Alpine inversion in northern Morocco. *Mémoires du Muséum national d'histoire naturelle*, *170*, 87-101.

Zizi M. (2002) Triassic-Jurassic extensional systems and their Neogene reactivation in Northern Morocco (the Rides Prerifaines and Guercif basin). Notes Mem Serv Géol Maroc 416:1-138.

Personal communication with:
Capella, W.
Dr. Eggenhuisen, J.
Dr. Krijgsman, W.
Dr. Matenco, L.C.
Dr. Trabucho Alexandre, J.
Tulbure, M.A.
de la Vera, A.
Dr. Wesseling, F.